NASA TECHNICAL NOTE

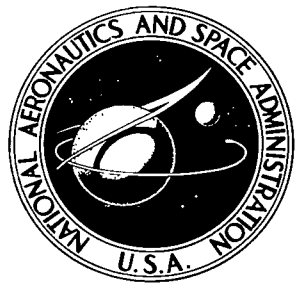

MEAN FLOW FIELD AND SURFACE HEATING PRODUCED BY UNEQUAL SHOCK INTERACTIONS AT HYPERSONIC SPEEDS

Stanley F. Birch and David H. Rudy

Langley Research Center
Hampton, Va. 23665

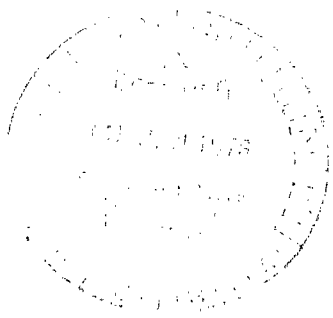

NATIONAL AERONAUTICS AND SPACE ADMINISTRATION • WASHINGTON, D. C. • DECEMBER 1975

1. Report No.	2. Government Accession No.	3. Recipient's Catalog No.
NASA TN D-8092		

4. Title and Subtitle

MEAN FLOW FIELD AND SURFACE HEATING PRODUCED BY UNEQUAL SHOCK INTERACTIONS AT HYPERSONIC SPEEDS

5. Report Date: December 1975

6. Performing Organization Code:

7. Author(s)

Stanley F. Birch and David H. Rudy

8. Performing Organization Report No.: L-10444

9. Performing Organization Name and Address

NASA Langley Research Center
Hampton, Va. 23665

10. Work Unit No.: 505-06-11-03

11. Contract or Grant No.:

12. Sponsoring Agency Name and Address

National Aeronautics and Space Administration
Washington, D.C. 20546

13. Type of Report and Period Covered: Technical Note

14. Sponsoring Agency Code:

15. Supplementary Notes

Stanley F. Birch: Former NASA-NRC Research Associate, now at the Boeing Commercial Airplane Co., Seattle, Wash.

16. Abstract

Mean velocity profiles were measured in a free shear layer produced by the interaction of two unequal strength shock waves at hypersonic free-stream Mach numbers. Measurements were made over a unit Reynolds number range of 3.77×10^6 per meter to 1.74×10^7 per meter based on the flow on the high velocity side of the shear layer. The variation in measured spreading parameters with Mach number for the fully developed flows is consistent with the trend of the available zero velocity ratio data when the Mach numbers for the data given in this study are taken to be characteristic Mach numbers based on the velocity difference across the mixing layer. Surface measurements in the shear-layer attachment region of the blunt-body model indicate peak local heating and static pressure consistent with other published data. Transition Reynolds numbers were found to be significantly lower than those found in previous data.

17. Key Words (Suggested by Author(s))

Compressible flow
Viscous flow
Supersonic flow
Free shear layers

18. Distribution Statement

Unclassified – Unlimited

Subject Category 34

19. Security Classif. (of this report)	20. Security Classif. (of this page)	21. No. of Pages	22. Price*
Unclassified	Unclassified	73	$4.25

*For sale by the National Technical Information Service, Springfield, Virginia 22161

MEAN FLOW FIELD AND SURFACE HEATING PRODUCED BY UNEQUAL SHOCK INTERACTIONS AT HYPERSONIC SPEEDS

Stanley F. Birch* and David H. Rudy
Langley Research Center

SUMMARY

Mean velocity profiles were measured in a compressible free shear layer produced by the interaction of two unequal strength shock waves at free-stream Mach numbers of 6.0 and 6.7. Measurements were made over a unit Reynolds number range of 3.77×10^6 per meter to 1.74×10^7 per meter based on the flow on the high velocity side of the shear layer. The measured spreading parameters for the flows in this study are consistent with the variation with Mach number of the available zero velocity ratio data when the Mach numbers of the present data are taken to be the characteristic Mach numbers based on the velocity difference across the mixing layer. The transition Reynolds numbers were found to be as much as a factor of 5 lower than results given in the data previously regarded as the most reliable for transition in free shear layers. Surface measurements in the shear-layer attachment region of the blunt-body model indicate peak local heating and static pressure consistent with other published data. Numerical predictions of the shear-layer flow were made using the Prandtl mixing length model with a streamwise effective viscosity factor in the transition region.

INTRODUCTION

The high local heating rates caused by shock interactions at hypersonic speeds have been the subject of numerous experimental and theoretical studies. In 1968 Edney (ref. 1) identified six basic types of shock interactions and measured associated local heat-transfer rates up to 10 times the local unperturbed free-stream values. This work showed that the severe local heating and high pressures are caused by the impingement of disturbances which emanated from the shock intersections. These disturbances can be shear layers, supersonic jets, or shocks; and the overall flow can be dominated by viscous and/or inviscid effects depending on the interaction geometry. Reference 1 summarizes work published before 1968 while details of more recent work are covered in references 2 to 6. Most of this work has been directed toward a better understanding

*Stanley F. Birch is a former NASA-NRC Research Associate and is presently at the Boeing Commercial Airplane Co., Seattle, Wash.

of the overall problem, concentrating on the effects of variations in gross properties such as Mach number, body geometry, impingement angle, and specific heat ratio. Limited study was also made of the viscous interactions themselves.

The present work is a detailed study of the flow field and the associated surface heating for the interaction geometry identified as type III by Edney. A type III interaction results when a weak extraneous shock impinges on the bow shock of a blunt body inside the sonic line. The type III interaction produces a single shear layer with supersonic flow on one side and subsonic flow on the other side. The high heating rates occur at the point where this shear layer attaches to the adjacent body; the rates depend critically on the width of the shear layer at the attachment point.

Previous experimental studies of surface heating and pressure in type III interactions have been made by Edney who used several types of blunt bodies (ref. 1) and by Hains and Keyes who used a hemisphere (refs. 2 and 3). Keyes and Morris (ref. 4) presented correlations of the data from references 2 and 3, showing that the surface heat transfer in the attachment region is highly dependent upon whether the shear layer is laminar or turbulent. Birch and Keyes (ref. 7) reported measured transition Reynolds numbers for the associated shear layers.

The present work is a study of the viscous mixing processes which determine the width of the shear layer. Shear-layer mean velocity profiles for several unit Reynolds numbers were experimentally determined in a type III interaction. In addition, surface oil-flow patterns, surface heat-transfer measurements, and shear-layer transition length measurements are presented.

SYMBOLS

a	speed of sound
c_p	specific heat at constant pressure
h	surface heat-transfer coefficient
ℓ	shear-layer length to transition point
M	Mach number
$M_{\Delta V}$	characteristic Mach number, $\frac{u_2 - u_3}{a_2}$
$N_{Re,T}$	transition Reynolds number, $\rho_2 u_2 \ell / \mu_2$

p	static pressure, N/m^2
p_o	tunnel total pressure, N/m^2
$p_{t,1}$	total pressure in region ahead of pitot probe shock wave, N/m^2
$p_{t,2}$	total pressure behind pitot probe shock wave $\left(p_{t,1} = p_{t,2} \text{ if } M < 1\right)$, N/m^2
T	static temperature, K
T_o	total temperature, K
u	streamwise velocity, m/sec
x	coordinate along surface of model from leading edge, cm
$\bar{x}$	streamwise coordinate (see fig. 25)
$\bar{x}_{TRANS}$	location of start of transition region
$\bar{x}_{TURB}$	location of start of turbulent region
y	coordinate normal to region 3 flow from model surface, cm
$\bar{y}$	$= y - y_{0.5}$
$y_{0.5}$	value of y where $\phi = 0.5$
α	angle of inclination of blunt-body model, deg
β	shock generator wedge angle, deg
γ_a, γ_b	streamwise effective viscosity factors
δ	shear-layer width
δ_{SL}	shear-layer width at attachment

θ_{SL} shear-layer angle relative to model surface inclination, deg

λ $= \dfrac{1 - \dfrac{u_3}{u_2}}{1 + \dfrac{u_3}{u_2}}$

μ dynamic viscosity

ρ density

σ spreading parameter

ϕ $= \dfrac{u - u_2}{u_3 - u_2}$

Subscripts:

av average value

peak maximum value

s surface value

w conditions based on measured surface temperature and peak surface static pressure

∞ free-stream conditions

1 conditions behind generator wedge shock

2,3 conditions on high and low velocity side of shear layer, respectively

4 conditions in region behind oblique shock at attachment point

APPARATUS AND TESTS

Test Facilities

The experimental investigation was conducted in the Langley 11-inch hypersonic tunnel and in the Langley 20-inch Mach 6 tunnel.

The nominal free-stream Mach number for the 11-inch facility is 6.8. The actual Mach number varied with total pressure and running time (ref. 8); however, this variation

produced no measurable effect on the shear-layer flow in these tests. The nozzle in this facility is two dimensional with a throat size of 0.236 cm by 27.9 cm with a core of uniform flow of approximately 15.2 cm by 15.2 cm in the test section. The usable Reynolds number range is from 0.16×10^7 per meter to 1.31×10^7 per meter with a mass flow of 5.44 kg/sec at a total pressure of 1.03 MN/m^2 and a total temperature of 590 K. Typical run times were 40 seconds.

The 20-inch Mach 6 tunnel is a blowdown facility described in the appendix of reference 9. The test Mach number was obtained with a fixed-geometry, two-dimensional contoured nozzle forming a throat section of 0.86 cm by 50.8 cm and a test section of 52.0 cm by 50.8 cm. The Reynolds number range was 2.3×10^6 per meter to 29.5×10^6 per meter with a maximum tunnel mass flow of 27 kg/sec. Tests were made in this facility to obtain data at higher Reynolds numbers than those attainable in the 11-inch tunnel. To give extended run times, i.e., 5 to 7 minutes in length, the tunnel flow was exhausted into the atmosphere using an annular air injector.

Models

The basic geometry used in this study is indicated in the schematic of the flow field for each tunnel shown in figure 1. A wedge set at a small angle relative to the flow was used to generate a weak planar shock wave which interacted with the bow shock of a suitably placed blunt body. Two different shock generator wedges were used in combination with two different blunt bodies.

The first set of models (shown in fig. 2) consisted of a 5^o shock generator wedge 15.2 cm wide by 44.4 cm long and a blunt body 6.35 cm wide by 6.26 cm long with an impingement surface angle of 30^o. This set of models was used for a preliminary study of the basic shock-interaction geometry. The results of this study indicated that because of crossflow on the low velocity side of the shear layer near the surface of the blunt body, it was difficult to calculate the positions of the resulting shocks accurately. A second set of models was therefore fabricated to overcome this difficulty.

This second set of models (shown in figs. 3(a) and 3(b)), which were used to obtain most of the detailed data reported here, had approximately the same dimensions as the first set, but the incident angles of both the shock generator wedge and the blunt body were adjustable. The models positioned in the test section are shown in figure 4. The blunt body, which was made from stainless steel, was fitted with 31 static-pressure orifices, 13 of which were located along the model center line 0.635 cm apart as shown in figure 5. The remaining 18 pressure taps were used to measure the off-center-line surface static-pressure field in the shear-layer attachment region. These pressure orifices were formed from 0.152-cm stainless steel tubing which was silver-soldered flush with the model surface. At the base of the model the tubes were connected to 1.22-m lengths

of 0.3175-cm outer diameter tubing; these tubes, in turn, were connected to pressure transducers outside the tunnel. A stycast resin blunt-body model identical in size and shape to the steel model was used for heat-transfer measurements and oil-flow studies.

Pressure Probes

Static-pressure probe.- The design of a suitable static-pressure probe for use in supersonic flows presents a number of difficulties resulting from the shock wave which forms at the tip of the probe. For a standard probe with a cylindrical body and a conical tip, the flow passing over the shoulder expands to below static pressure and recompresses to true static pressure further down the probe body. In the standard design the static-pressure orifices must be located 15 to 20 probe diameters back from the tip. Use of the smallest practical probe-body diameter would have resulted in a probe length too long to be practical for local static-pressure measurements in the present flow field. The probe actually used is shown in figure 6. Unpublished tests on a larger probe of similar design indicated that at Mach numbers up to 2.0, the probe generally senses pressures larger than true static; however, errors are less than 1 percent when the probe axis is alined with the local flow direction. Effects of probe inclination generally serve to reduce the probe-sensed pressure by amounts which vary with both inclination and Mach number. In general, static-pressure errors associated with the probe itself were less than 2 percent for inclinations up to approximately 12°, 8°, and 4° at Mach numbers of 0.6, 1.1, and 2.0, respectively.

Pitot pressure probes.- The tip of the probe used in the 11-inch tunnel tests was made from 0.153-cm outer diameter stainless steel tubing flattened to give an opening about 0.00508 cm high. The same probe was used at all data stations. Four probes of appropriate length were used in the 20-inch tunnel tests with one probe for each of the four data stations. The tips of these probes were made from 0.1016-cm outer diameter thin-wall stainless steel tubing flattened to give an opening about 0.02032 cm high.

Test Conditions

The 11-inch tunnel data were obtained at nominal tunnel stagnation pressures p_0 of 5 atm and 10 atm (1 atm = 101.325 kN/m^2) with an average stagnation temperature of 617 K. The unit Reynolds numbers based on the flow on the high velocity side of the shear layer (region 2) were 3.8×10^6 per meter and 7.5×10^6 per meter for total pressures of 5 and 10 atm, respectively.

To obtain data on the spreading rate of a shear layer at Reynolds numbers larger than were possible in the 11-inch tunnel, two further series of tests were run in the 20-inch Mach 6 tunnel. The first series were run with a nominal tunnel stagnation pressure p_0 of 1.03 MN/m^2 to provide approximate overlap with the 11-inch results. The

average stagnation temperature for these tests was 461 K. Therefore, the unit Reynolds number based on the flow on the high velocity side of the shear layer (region 2) was 1.74×10^7 per meter.

The second series of tests in the 20-inch tunnel were run at a nominal tunnel stagnation pressure p_o of 3.45 MN/m^2 and at an average total stagnation temperature T_o of 489 K. These conditions gave a unit Reynolds number of 4.99×10^7 per meter; the value is approximately 6.6 times higher than the highest value run in the 11-inch tunnel.

RESULTS AND DISCUSSION

Preliminary Schlieren Flow Field Studies

The type III interaction (see ref. 1) described here results when a weak extraneous shock intersects a strong shock. The strong shock was the bow shock of a blunt body and the geometry of the interaction shown in figure 1 is uniquely determined by M_∞, M_1, and β provided that the interaction takes place upstream of the sonic line. The geometry of the interaction may be calculated using the heart diagram described in reference 1 or numerically, using the procedure given in reference 10. In the present study both methods were used; each provided essentially the same results. Since the interaction geometry is independent of its position, the blunt body may be designed to insure that the shock between regions 1 and 2 is straight. Note, however, that because of the subsonic flow region between the shock and the blunt body, the angle between the surface and the shock is not that computed for a two-dimensional wedge. In this study the shock was nearly parallel to the surface. This was caused primarily by the crossflow in the low velocity side of the shear layer.

One of the objectives of the preliminary study was to optimize the geometry to give the maximum length of shear layer with minimum three-dimensional effects. These requirements were subject to a total blockage limit for the 11-inch tunnel; this limit restricted the model sizes which could be used. The arrangement shown in figure 4 was found to be nearly optimum. If the blunt body is moved further back, the separated boundary layer from the shock generator wedge interferes with the reattachment region of the shear layer. If the blunt body is moved forward, the gap between the models decreases, restricting the flow in this region and increasing the three-dimensional effects. Eventually the boundary layer on the shock generator wedge separates, and together with the separation shock impinges on and disrupts the flow in the region of the original shock interaction. In order to maximize the separation of the models, this shock interaction was located close to but inside the sonic line on the blunt body. However, the configuration could not be adjusted too finely without unduly complicating the experimental study because of small changes in the interaction geometry with Reynolds

number. This change was caused mainly by a decrease in the boundary-layer displacement thickness on the shock generator wedge with increasing unit Reynolds number; this change moved the interaction point farther from the blunt body.

The spark schlieren photographs (figs. 7(a) to 7(c)) show some typical results from these preliminary studies. In figure 7(a), the separation distance between the two models is too large, allowing the separated boundary layer from the shock generator wedge to disrupt the flow field of interest. For the configuration shown in figure 7(b), the gap between the models and the shock generator wedge angle were both decreased; thus, the separated-boundary-layer interference moved further toward the base of the blunt body. In figure 7(c), the bases of the models are alined, eliminating the interference. As mentioned previously, however, three-dimensional effects are increased in this configuration.

For the 11-inch $(M_\infty = 6.7)$ tunnel data tests, the second set of models was used. A schematic of the flow field is shown in figure 1(a). To maintain approximately the same values for M_2 and M_3 in the $M_\infty = 6$, 20-inch tunnel, the shock generator wedge angle was adjusted to 11°. A sketch of the resulting flow field is shown in figure 1(b).

Figures 8(a) to 8(c) show spark schlieren photographs from the 11-inch tunnel tests for three unit Reynolds numbers. As the unit Reynolds number increases, the region of laminar flow in the shear layer decreases. The photograph in figure 8(d) was taken with the schlieren system knife edge adjusted to indicate better the shear-layer attachment which occurs near the base of the blunt-body model.

Figures 8(e) to 8(g) show spark schlieren photographs from the Mach 6, 20-inch tunnel tests for three unit Reynolds numbers. Note that some of these schlieren photographs show clear dark and light bands at angles of approximately 45° with respect to the main flow direction. These bands appear to be similar to some of the photographs in reference 11 and suggest a distinct large eddy structure. However, because of the large variation observed among photographs in a series of photographs from a given run, this large eddy structure appears to be strongly intermittent.

Attempts were made to reduce three-dimensional effects by fitting side plates to the blunt body. It was found, however, that the resulting increase in blockage separated the boundary layer on the shock generator wedge and disrupted the flow field. The extent of the remaining three-dimensionality and its possible effect on the flow is discussed in more detail later.

Static-Pressure Measurements

Surface static-pressure measurements.- Figure 9 shows the variation in static pressure along the center line of the model for several angles of inclination α of the

model. It was found that the static pressure was very sensitive to the relative position of the models and some small differences in the static-pressure distributions were noted for different tests using nominally the same configuration. Figure 10 shows the center-line static-pressure distribution at 5 atm and 10 atm for the model configuration used during the 11-inch tests. Figure 11 shows the surface static-pressure variation in the cross plane normal to the center line at $x = 5.21$ cm from the 11-inch tests. The pressure is constant in the central region about the center line with a slight symmetrical dropoff near the edges of the model.

Static-pressure profiles.- The static-pressure profiles shown in figure 12 were obtained using the static-pressure probe described previously. It can be seen that each profile consists of two sets of data: one set taken with the static-pressure probe alined with the flow on the high velocity side of the shear layer and the other set taken with the probe body parallel to the blunt-body surface. By assuming that the latter data were more accurate on the low velocity side of the shear layer where the flow on the center line is expected to be parallel to the surface, it was possible to estimate the actual static-pressure profile. The agreement between surface static-pressure measurements and those measurements made with the static probe in the subsonic region of the flow seems to support this assumption.

Oil Flow

The oil-flow pattern on the surface of the blunt body is shown in figure 13. To avoid the danger of blocking the static-pressure orifices on the steel model, the oil-flow patterns were obtained by using the stycast heat-transfer model. Visualization was accomplished by putting an irregular pattern of oil drops on the model surface.

The appearance of the oil pattern after a run is shown in figure 13. Two regions of oil accumulation can be clearly seen. The oil accumulation on the nose of the model is caused by the stagnation of the streamlines coming through the normal bow shock. The reason for the second region of oil accumulation, located above the nose on the flat portion of the model surface, is less obvious; however, the accumulation is not the result of the stagnation of streamlines in the boundary layer on the surface. The small adverse static-pressure gradient accelerates the growth of the boundary layer on the blunt body and reduces the axial velocity close to the surface. This gradient, combined with the crossflow which results from the transverse static-pressure gradient, leads to increasing angles between streamlines close to the surface and the center line of the blunt body as the attachment point is approached. However, the axial velocity at the attachment point is still large enough to avoid stagnation or reverse flow in the boundary layer. Downstream of the attachment point, the angles between the streamlines and the blunt-body center line again decrease as the velocity of the flow close to the surface increases.

The low axial static-pressure gradients observed in the tests described here result primarily from the small angle between the attaching shear layer and the model surface. As this angle increases, the adverse static-pressure gradient also increases (fig. 9). For flow geometries where the angle between the shear layer and the surface is large (for example, refs. 1 and 3), a region of reverse flow is generally observed between the shear layer and the surface upstream of the attachment point. There is no such reverse flow in the flow field used in this study.

Mean Velocity Profiles

The mean velocity data were obtained from pitot pressure traverses of the mixing layer. For all tests the pitot probe was approximately alined with the flow on the high velocity side of the shear layer. Traverses were then made at right angles to this direction.

The estimated static-pressure profiles (fig. 12) were used to obtain velocity data from the pitot data assuming constant total temperature for the 11-inch center-line profiles at $p_o = 10$ atm. In all other cases, however, it was assumed that the static pressure in the shear layer equaled the surface value at the particular x station. As shown by the results given in figure 12, this assumption is reasonable for the low velocity region. In the supersonic region the velocity is only slightly affected by small changes in static pressure. Overall the assumption has a negligible effect on the values of the shear-layer spreading rate.

Center-line data, 11-inch tunnel.- Center-line velocity (u/u_2) profiles ahead of the attachment region are presented in tables I and II, are plotted in figure 14, and exhibit the usual "error function" shapes. (Each profile is a composite of several tunnel runs.) Plots of lines of constant ϕ (fig. 15) indicate that there is a substantial difference in the spreading rate for the two flows. The spreading parameter σ for the 10-atm flow was calculated to be 30, while at 5 atm the shear layer appears to be spreading approximately 50 percent faster, although in this case the spreading rate is not strictly linear. Hence no σ can be computed for the 5-atm flow. The spreading parameter σ is defined as

$$\sigma = \frac{1.804(X_B - X_A)}{Y_B - Y_A} \tag{1}$$

where Y_A and Y_B are the lateral distances between points for which ϕ is 0.1 and 0.9 at longitudinal stations X_A and X_B, respectively. The numerical constant is based on a comparison between the data and the error function profile (fig. 3.1 of ref. 12) which was found to be the best approximation of the present experimental results.

Off-center-line data, 11-inch tunnel.- Figure 16 shows profiles for $x = 5.21$ cm at locations 1.27 cm away from the center line on each side. Comparison of these profiles with the center-line profile at the same x location shows that the three profiles are almost identical. The data presented in figure 16 are tabulated in table III. Each of these profiles is a composite of several tunnel runs.

Center-line data, 20-inch tunnel.- Normalized center-line velocity (u/u_2) profiles ahead of the attachment region for $p_0 = 1.03$ MN/m^2 are presented in table IV and plotted in figure 17. A plot of lines of constant ϕ is given in figure 18. The calculated spreading parameter for this flow was $\sigma = 26$. Equation (1) was used to compute σ.

Normalized center-line velocity profiles for the $p_0 = 3.45$ MN/m^2 runs are plotted in figure 19 with the tabulated data given in table V. A plot of constant velocity lines is given in figure 20. During this high Reynolds number test, the probe designed for the $x = 4.19$ cm station was irreparably damaged, and the longer probe for the $x = 3.43$ cm station was used as a substitute. Analysis of the data and of schlieren photographs taken during the tests indicated that the probe experienced a deflection under the high aerodynamic load while traversing the supersonic region at this station; therefore, the probe position was altered from the indicated reading. Because of this problem, the data obtained at this station, particularly in the supersonic region of the shear layer, are not considered to be reliable. Therefore the lines of constant ϕ in figure 20 are biased toward the two downstream stations. The resulting σ again based on the error function profile was calculated to be 28.0 (using eq. (1)).

Discussion of mean velocity results.- To establish a common basis for comparing the present results with other published data for supersonic shear layers, the spreading rates calculated from the present data were extrapolated to the values they would have in a shear layer with a zero velocity ratio, i.e., $u_3/u_2 = 0$. This was accomplished by assuming that the variation of σ with velocity ratio established for subsonic flows, i.e., $\sigma\lambda$ = constant, where

$$\lambda = \frac{1 - \frac{u_3}{u_2}}{1 + \frac{u_3}{u_2}}$$

is applicable to the present results. Since the observed variation of σ with velocity ratio in subsonic flows appears to follow from simple relativistic considerations and implies no change in the basic turbulent mixing process, this assumed variation appears to be reasonable.

As a first approximation, the lateral spreading rate of a mixing layer is proportional to the velocity difference across the layer $(u_2 - u_3)$ while the axial convection velocity is proportional to the average velocity in the layer $(u_3 + u_2)/2$. Therefore, the angular spreading rate of the mixing layer is expected to be proportional to the ratio of these two quantities. Since their relative magnitudes change with velocity ratio, the resulting change in angular spreading rate of the mixing layer should be proportional to $(u_2 - u_3)/(u_2 + u_3)$ if the basic turbulent mixing process does not change as the velocity ratio changes. However, since the spreading rate in a supersonic shear layer is Mach number dependent (paper 2 of ref. 13), it is also necessary to define a characteristic Mach number corresponding to that used for shear layers with zero velocity ratios. The velocity difference across the mixing layer is clearly the characteristic velocity for the flow; therefore, the characteristic Mach number is defined here as $(u_3 - u_2)/a_2$ where a_2 is the speed of sound on the high velocity side of the shear layer. Note that the static temperature difference across the present mixing layer is not the same as for a zero velocity ratio mixing layer with the same nominal Mach number and a constant total temperature. This difference, however, is small here and can probably be ignored without serious error. Certainly, for subsonic flows the best available data (ref. 14) indicate that density variations, as such, have only a small effect on the mixing rate. In reference 15 it was shown that a variation of from 1.0 to 1.3 in total temperature ratio across a Mach 4 mixing layer did not produce a measurable change in the mixing rate. Nevertheless, the available experimental data are very limited and this result should not be extrapolated too far. A direct determination of the variation of spreading rate with velocity ratio for supersonic flows would, of course, be preferable, but no such data appear to be available at present.

The $\sigma\lambda$ values at the characteristic Mach numbers for the present tests are plotted in figure 21 with data from references 15 to 30 for zero velocity ratio ($\lambda = 1$) shear layers. (Only data at highest Reynolds number are shown for each tunnel.) An error band of ±10 percent is indicated for the present data. The variation in the spreading rate of the mixing layers with Mach number appears to agree with that recommended in paper 2 of reference 13 for fully developed supersonic shear layers.

The higher spreading rate of the low Reynolds number flow $(p_o = 5 \text{ atm})$ is in agreement with the findings of Morrisette and Birch (see ref. 30) who reported that the spreading rate of a shear layer in the near field of a Mach 5 jet increased significantly when the Reynolds number was decreased. They attributed this difference in spreading rate to low Reynolds number effects, indicating that their low Reynolds number flow was not fully developed. Low Reynolds number effects are also discussed by Birch and Eggers (paper 2 of ref. 13). While the present results suggest a similar conclusion, the result is less definitive here because of the close proximity of the shear layer to the model surface. Surface static-pressure measurements on the blunt body show a symmetric drop

in static pressure of 10.3 kN/m^2 and 17.2 kN/m^2, respectively, for 5 and 10 atm between the center line and near the model edge. Although this static-pressure gradient indicates some crossflow, its low level suggests that the three-dimensional effects are probably confined to the low velocity side of the shear layer close to the blunt body. It should also be noted that while the shear stress levels in a radial free jet (ref. 31) and a radial wall jet (ref. 32) are approximately twice as large as the levels in the corresponding two-dimensional flows, there is little change in the overall spreading rate. There is, therefore, no a priori reason for believing that a small crossflow would substantially alter the spreading rates in the present shear layers if the flows of this study were fully developed.

In the present experiments the initial thickness of the shear layer is very small (same order of magnitude as the shock thickness). The apparent persistence of low Reynolds number effects up to at least 5 atm in the results given here suggests that the appropriate criterion for the length required for the flow to become fully developed should be a function of Reynolds number rather than of some number of initial boundary-layer thicknesses. This conclusion agrees with the results found by Bradshaw (ref. 33) for subsonic shear layers.

Transition Data

The transition results for free shear layers presented in figure 22 are based on the present study in the 11-inch tunnel and on data from reference 3. The latter data were taken in the Langley 20-inch tunnel (Mach 6) using a hemisphere-cylinder blunt body 5.08 cm in diameter. Further details of the apparatus used in this study are presented in reference 3. The transition length used here is defined as the length along the shear layer from the shock interaction to the point at which turbulence becomes visible on schlieren photographs. An average value of ℓ based on a series of photographs was used to determine the transition Reynolds number $N_{Re,T}$; these results are given in table VI.

Most of the published results on transition in free shear layers are based on shear layers with a velocity u_3 of zero or close to zero. For the present work, the velocity ratio u_3/u_2 is substantial $\left(u_3/u_2 \neq 0\right)$; consequently, its effects cannot be ignored. If these results are to be compared with previously published data obtained for separation geometries where $u_3 \approx 0$, it is necessary to extrapolate the measured values of $N_{Re,T}$ to the values they would have for a zero velocity ratio. Since the literature contains no experimental results for the variation of $N_{Re,T}$ with the velocity ratio u_3/u_2, it was suggested in reference 1 that, as a first approximation, the following assumption be made

$$N_{Re,T,0} = \lambda N_{Re,T} \tag{2}$$

where $N_{Re,T,0}$ is the value of $N_{Re,T}$ when $u_3 = 0$. The quantity $N_{Re,T}$ is defined as

$$N_{Re,T} = \frac{\rho_2 u_2 \ell}{\mu_2} \tag{3}$$

The lambda dependence in equation (2) is similar to that used for the variation of the shear-layer spreading rate with velocity ratio and is based on the assumption that the characteristic velocity describing the transition process is the velocity difference between the two streams. Note further that for given values of $u_2 - u_3$ and M_2, the transition length must increase with u_2 and u_3 simply because of the increase in the average convection velocity in the shear layer. As stated in reference 7, equation (2) ignores the dependence of $N_{Re,T}$ on M_3, an assumption which cannot be expected to hold when the velocity on both sides of the shear layer is supersonic. In reference 7, $N_{Re,T}$ was plotted against M_2; however, in view of the results presented in the discussion of the spreading rates, it is more appropriate to plot $N_{Re,T}$ against the Mach number based on the velocity difference across the shear layer as in figure 22.

While all the transition data in figure 22 show a similar trend with Mach number, it should be noted that the data from reference 34 are based on conditions ahead of the separation shock rather than on local values, and the data from reference 35 are for separated axisymmetric rather than planar boundary layers. From the limited results of references 34 and 35 on transition in separated boundary layers, Edney (ref. 1) concluded that the correlation of transition Reynolds number with Mach number given by Chapman, et al. (ref. 34) was valid for shear layers produced by type III interactions. The results of this study do not justify this conclusion but show that predictions of length to transition based on this correlation can be in error by as much as a factor of 5.

Surface Heating

Heat-transfer data were obtained in the 11-inch tunnel for $p_0 = 5$ atm and $p_0 = 10$ atm using the phase-change coating technique (ref. 36). The 11-inch tunnel was not equipped with an injection system; therefore, the model was exposed to the flow during the short time the tunnel total temperature and total pressure were rising to steady-state values. Only data taken at times at least twice the length of the tunnel total-temperature transient were used since calculations showed that such data were relatively unaffected by the short transient. (The calculated surface heat-transfer coefficient h varied less than 5 percent from the value for constant total temperature for long melt times.) In addition, the data reduction method of Hunt, et al. (ref. 37) was used. Their method incorporates into the solution the measured total-temperature variation. The overall error associated with the data reduction procedure is estimated to be no more than 10 to 15 percent.

The surface center-line heat-transfer coefficient data in the attachment region are shown in figure 23. Since the heating data for each total pressure represent measurements from several runs, the scatter in the data is attributed to slight variations in test conditions between these runs. The peak value of h is 6 percent higher at 10 atm than at 5 atm with the peak occurring at an x 0.635 cm further back on the model surface at 10 atm. This difference is partially caused by a change in location of the shock interaction produced by a difference in boundary-layer displacement thickness on the shock generator wedge at the lower unit Reynolds number. This changes slightly the angle of the impinging shock wave; hence, the interaction location.

These data are compared with the turbulent data of reference 3 in figure 24 where measured peak Stanton number $h_{peak}/(\rho_w u_4 c_p)$ is plotted as a function of Reynolds number based on shear-layer thickness at attachment δ_{SL}, $(\rho_w u_4 \delta_{SL})/(\mu_w \sin \theta_{SL})$. (It should be noted that the Keyes-Hains (ref. 3) data shown in figure 24 have been revised by Keyes in an unpublished study after a reinterpretation of photographs from the original tests had been made.) The density ρ_w and the viscosity μ_w are based on measured surface temperature and measured peak static pressure. The value θ_{SL} is the shear-layer angle relative to model surface inclination. The velocity u_4 in the region behind the oblique shock usually occurs at the attachment point. (See fig. 5 of ref. 3.) In the present study, the attachment occurred near the base of the model and no oblique shock resulted. Therefore, an approximation to u_4 was computed using u_2 and assuming an oblique shock at the attachment point with flow parallel to an extended model surface behind the shock. The Keyes-Hains data and correlation represent shear layers which are three dimensional in nature with relatively large (27^o to 42^o) attachment angles. Also shown is the correlation of Bushnell and Weinstein (ref. 38) for reattaching two-dimensional turbulent boundary layers. This correlation, in general, represents data at relatively low attachment angles The data presented here with an intermediate value of θ_{SL} (18.6^o) and some three-dimensional effects fall between these two correlations, indicating perhaps that the 10-atm flow is less influenced by three-dimensional effects than the 5-atm flow.

NUMERICAL PREDICTIONS

Even at high Reynolds number, when transition from laminar to turbulent flow takes place close to the shock interaction, the shear layer does not achieve a constant spreading rate until far downstream. It was not possible to take detailed velocity-profile data over the initial region because of the small width of the mixing layer there. It was, however, possible to estimate the effective viscosity over this region. If the effective viscosity is assumed to be equal to the sum of the laminar and turbulent viscosities, then in general, $\mu_{effective}$ can be written as

$$\mu_{effective} = \mu_{laminar} + \gamma\mu_{turbulent} \tag{4}$$

The function γ is a streamwise "intermittency" factor introduced to simulate the variation of the effective viscosity in the transition region. The function is 0 for laminar flow and 1.0 for fully developed turbulent flow.

Numerical calculations were made using the quasi-parallel solution technique of reference 39. The Prandtl mixing length model (see paper 4 of ref. 13) was used to model the turbulent viscosity; i.e.,

$$\mu_{turbulent} = \rho\left(\frac{\ell}{\delta}\right)^2\delta^2\left|\frac{\partial u}{\partial y}\right|\frac{\partial u}{\partial y} \tag{5}$$

where δ is the width of the mixing region and ℓ/δ is the so-called mixing-length constant. Figure 25 shows two possible γ functions which were used in the calculation. Qualitatively these functions were chosen to be similar to the variation in shear stress in the transition found by Bradshaw (ref. 33) for subsonic shear layers. In these calculations the locations of the beginning and the end of the transition region were estimated.

Two series of calculations were performed for conditions corresponding to the p_o = 10 atm, 11-inch tunnel case. The results are shown in figure 26 together with the experimental data for two streamwise locations. The mixing-length constant was taken to be $\ell/\delta = 0.064$. This value was estimated to give a σ of 16 at Mach 1.6 based on the mixing-length predictions for two-dimensional free shear layers in paper 4 of reference 13. The calculations were started with a profile 0.06 cm wide since the computer code would not accept a step profile, i.e., a zero-width profile. As shown in figure 26 with $\gamma = 1$ and $\ell/\delta = 0.064$, the width of the mixing layer is underpredicted at both profile stations; i.e., the shear layer mixes too slowly. Use of a value of $\gamma = 0$ in the laminar region and a value of $\gamma = 1.0$ in the fully turbulent region implies that γ must be greater than 1.0 over much of the transition region, if the width of the mixing region is to be predicted correctly at the two selected locations. The results shown in figure 26 suggest that a variation of effective viscosity close to that given by the γ_b curve of figure 25 probably best represents the actual variation of the effective viscosity in the transition region. Note that this variation implies that there is an initial overshoot in the effective viscosity followed by a slow relaxation to the equilibrium value. While these results cannot be regarded as definitive, they are consistent with other published results. Qualitatively the results suggest a variation in shear stress in the transition region very similar to that found by Bradshaw (ref. 33) for subsonic shear layers. They also offer an explanation for the discrepancy between low and high Reynolds number data for supersonic shear layers reported in reference 13. Because of the initial overshoot in viscosity, the average effective viscosity over the transitional region is higher than the asymptotic

value. This effect, compounded by an apparent increase in the Reynolds number required to achieve fully developed flow in supersonic shear layers and the absence of turbulence data, gave little variation in spreading rate with Mach number for low Reynolds number flow. High Reynolds number shear layers, on the other hand, show a significant decrease in mixing rate with Mach number.

CONCLUDING COMMENTS

Before numerical methods for solving the boundary-layer equations became generally available, much effort was expended in developing analytic methods for dealing with the nonsimilar region of a free shear layer, where its velocity profile changed from a wall boundary-layer shape at the separation point to an error-function shape further downstream. In recent years it has become clear that this problem is only one of those which must be faced in attempting to predict the downstream development of a separated boundary layer. If the initial boundary layer is laminar, or if the shear layer is generated by a shock interaction, this developing region includes a transition from laminar to turbulent flow. Although the problem of predicting transition is generally ill-posed, the resulting practical problems are often less severe than for the corresponding problem in wall boundary layers. This difference results because the strong inflectional instabilities encountered in free shear flows induce turbulence at low Reynolds numbers and significant regions of laminar flow are seldom encountered in full-scale high Reynolds number flows. However, the shear layer does not reach its asymptotic spreading rate until far downstream of this transition point, even in the absence of complications such as adverse pressure gradients. The peak shear stress in this transitional region can vary widely, and values of up to twice the asymptotic level have been measured in subsonic flows. A similar variation can be inferred for supersonic flows from the reported variation of spreading rate of the mixing layer with Reynolds number.

In supersonic free shear flows the problem is further complicated by an apparent variation in the asymptotic spreading rate with Mach number for Mach numbers greater than one. At present the mechanism responsible for this effect is not well understood, although Oh (ref. 40) has recently proposed a possible explanation. A major problem is the lack of reliable experimental data, particularly turbulence data. The effect itself, however, has very important practical implications at high Mach numbers. Since the transition Reynolds number and the Reynolds number required to achieve fully developed flow both appear to increase with Mach number, the likelihood of significant differences between model-scale and full-scale data increases also with Mach number. These differences occur since it becomes progressively more difficult to reproduce full-scale Reynolds numbers in a wind tunnel as the Mach number of the flow increases. A shear layer which is laminar or transitional on a wind-tunnel model at hypersonic speeds will

probably be fully developed at full scale. This fact can lead to significant discrepancies between model-scale and full-scale shock interference heating data, and under some conditions the heating at full scale can be much more severe than model-scale experiments indicate.

Although the results presented here for the fully developed regions of the shear layer appear to be consistent with previously reported results, and therefore, may be predictable, there appears to be no reliable method of predicting the developing region of the shear layer. This situation is unlikely to improve significantly until more and better data become available. For some specific recommendations the reader is referred to papers 20 and 21 of reference 13.

SUMMARY OF RESULTS

In the present investigation mean velocity-profile data were obtained for compressible free shear layers produced by the interaction of two unequal strength shock waves. Tests were made in two wind tunnels with free-stream Mach numbers of 6.7 and 6.0 over a unit Reynolds number range of 3.77×10^6 per meter to 1.74×10^7 per meter based on the flow on the high velocity side of the shear layer. The following results were obtained:

1. The measured spreading parameters for these shear layers were found to be consistent with previous data when the Mach numbers for the present data are taken to be characteristic Mach numbers based on the velocity difference across the shear layer.

2. Transition Reynolds numbers were found to be a factor of 5 lower than those previously regarded as the most reliable data for transition in free shear layers.

3. Surface measurements in the shear-layer attachment region of the blunt-body model indicate peak local surface heating and surface static pressure consistent with other published data.

4. Numerical predictions of the flow were made using the Prandtl mixing length turbulence model. A streamwise effective viscosity factor was included in the transition region to improve the prediction.

Langley Research Center
National Aeronautics and Space Administration
Hampton, Va. 23665
October 21, 1975

REFERENCES

1. Edney, Barry: Anomalous Heat Transfer and Pressure Distributions on Blunt Bodies at Hypersonic Speeds in the Presence of an Impinging Shock. FFA Rep. 115, Aeronaut. Res. Inst. of Sweden, 1968.

2. Hains, F. D.; and Keyes, J. Wayne: Shock Interference Heating in Hypersonic Flows. AIAA J., vol. 10, no. 11, Nov. 1972, pp. 1441-1447.

3. Keyes, J. Wayne; and Hains, Frank D.: Analytical and Experimental Studies of Shock Interference Heating in Hypersonic Flows. NASA TN D-7139, 1973.

4. Keyes, J. Wayne; and Morris, Dana J.: Correlations of Peak Heating in Shock Interference Regions at Hypersonic Speeds. J. Spacecraft & Rockets, vol. 9, no. 8, Aug. 1972, pp. 621-623.

5. Keyes, J. Wayne: Off-Center-Line Shock-Interference Heating Patterns on Basic Shapes in Hypersonic Flows. NASA TM X-2866, 1973.

6. Craig, Roger H.; and Ortwerth, Paul J.: Experimental Study of Shock Impingement on a Blunt Leading Edge With Application to Hypersonic Inlet Design. AFAPL-TR-10, U.S. Air Force, Apr. 1971. (Available from DDC as AD 726 111.)

7. Birch, Stanley F.; and Keyes, J. Wayne: Transition in Compressible Free Shear Layers. J. Spacecraft & Rockets, vol. 9, no. 8, Aug. 1972, pp. 623-624.

8. McLellan, Charles H.; Williams, Thomas W.; and Beckwith, Ivan E.: Investigation of the Flow Through a Single-Stage Two-Dimensional Nozzle in the Langley 11-Inch Hypersonic Tunnel. NACA TN 2223, 1950.

9. Goldberg, Theodore J.; and Hefner, Jerry N. (with appendix by James C. Emery): Starting Phenomena for Hypersonic Inlets With Thick Turbulent Boundary Layers at Mach 6. NASA TN D-6280, 1971.

10. Morris, Dana J.; and Keyes, J. Wayne: Computer Programs for Predicting Supersonic and Hypersonic Interference Flow Fields and Heating. NASA TM X-2725, 1973.

11. Yule, A. J.; Bruun, H. H.; Baxter, D. R. J.; and Davies, P. O. A. L.: Structure of Turbulent Jets – Second Annual Report Time Domain Analysis of Turbulent Structure. Memo. No. 506, Inst. Sound & Vib. Res., Univ. Southhampton, Mar. 1974.

12. Halleen, R. M.: A Literature Review on Subsonic Free Turbulent Shear Flow. AFOSR-TR-5444, U.S. Air Force, Apr. 1964. (Available from DDC as AD 606 758.)

13. Free Turbulent Shear Flows. Volume I – Conference Proceedings. NASA SP-321, 1973.

14. Brown, Garry L.; and Roshko, Anatol: On Density Effects and Large Structure in Turbulent Mixing Layers. J. Fluid Mech., vol. 64, pt. 4, July 1974, pp. 775-816.

15. Sirieix, M.; and Solignac, J. L.: Contribution a l'Etude Experimentale de la Couche de Melange Turbulent Isobare d'un Encoulement Supersonique. Separated Flows, Pt. I, AGARD CP No. 4, May 1966, pp. 241-270.

16. Tollmien, Walter: Calculation of Turbulent Expension Processes. NACA TM 1085, 1945.

17. Cordes, G.: Untersuchungen zur statischen Druckmessung in turbulenter Strömung. Ing.-Arch., Bd. VIII, Heft 4, Aug. 1937, pp. 245-270.

18. Reichardt, Hans: Gesetzmässigkeiten der freien Turbulenz. VDI-Forschungsh. 414, 1942.

19. Liepmann, Hans Wolfgang; and Laufer, John: Investigations of Free Turbulent Mixing. NACA TN 1257, 1947.

20. Gooderum, Paul B.; Wood, George P.; and Brevoort, Maurice J.: Investigation With an Interferometer of the Turbulent Mixing of a Free Supersonic Jet. NACA Rep. 963, 1950. (Supersedes NACA TN 1857.)

21. Bershader, D.; and Pai, S. I.: On Turbulent Jet Mixing in Two-Dimensional Supersonic Flow. J. Appl. Phys., vol. 21, no. 6, June 1950, pp. 616.

22. Crane, L. J.: The Laminar and Turbulent Mixing of Jets of Compressible Fluid. Pt. II – The Mixing of Two Semi-Infinite Streams. J. Fluid Mech., vol. 3, pt. I, Oct. 1957, pp. 81-92.

23. Johannesen, N. H.: Further Results on the Mixing of Free Axially-Symmetrical Jets of Mach Number 1.40. R. & M. No. 3292, Brit. A.R.C., 1962.

24. Maydew, R. C.; and Reed, J. F.: Turbulent Mixing of Axisymmetric Compressible Jets (in the Half-Jet Region) With Quiescent Air. SC-4764 (RR), Sandia Corp. (Albuquerque, N. Mex.), Mar. 1963.

25. Rhudy, J. P.; and Magnan, J. D., Jr.: Turbulent Cavity Flow Investigation at Mach Numbers 4 and 8. AEDC-TR-66-73, U.S. Air Force, June 1966. (Available from DDC as AD 483 748.)

26. Eggers, James M.: Velocity Profiles and Eddy Viscosity Distributions Downstream of a Mach 2.22 Nozzle Exhausting to Quiescent Air. NASA TN D-3601, 1966.

27. Wyganski, I.; and Fiedler, H.: Some Measurements in the Self-Preserving Jet. J. Fluid Mech., vol. 38, pt. 3, Sept. 18, 1969, pp. 577-612.

28. Hill, W. G., Jr.; and Page, R. H.: Initial Development of Turbulent, Compressible, Free Shear Layers. Trans. ASME, Ser. D: J. Basic Eng., vol. 91, no. 1, Mar. 1969, pp. 67-73.

29. Ikawa, Hideo: Turbulent Mixing Layer Experiment in Supersonic Flow. Ph. D. Thesis, California Inst. of Technol., 1973.

30. Morrisette, E. Leon; and Birch, Stanley F.: Mean Flow and Turbulence Measurements in a Mach 5 Shear Layer. Pt. I – The Development and Spreading of the Mean Flow. Fluid Mechanics of Mixing, Earl M. Uram and Victor W. Goldschmidt, eds., American Soc. Mech. Eng., c.1973, pp. 79-86.

31. Heskestad, Gunnar: Hot-Wire Measurements in a Radial Turbulent Jet. Trans. ASME, Ser. E: J. Appl. Mech., vol. 33, no. 2, June 1966, pp. 417-424.

32. Bradshaw, Peter: Variations on a Theme of Prandtl. Turbulent Shear Flows, AGARD-CP-93, Jan. 1972, pp. C-1 – C-10.

33. Bradshaw, P.: The Effect of Initial Conditions on the Development of a Free Shear Layer. J. Fluid Mech., vol. 26, pt. 2, Oct. 1966, pp. 225-236.

34. Chapman, Dean R.; Kuehn, Donald M.; and Larson, Howard K.: Investigation of Separated Flows in Supersonic and Subsonic Streams With Emphasis on the Effect of Transition. NACA Rep. 1356, 1958.

35. Crawford, Davis H.: Investigation of the Flow Over a Spiked-Nose Hemisphere-Cylinder at a Mach Number of 6.8. NASA TN D-118, 1959.

36. Jones, Robert A.; and Hunt, James L.: Use of Fusible Temperature Indicators for Obtaining Quantitative Aerodynamic Heat-Transfer Data. NASA TR R-230, 1966.

37. Hunt, James L.; Pitts, Joan I.; and Richie, Christine B.: Application of Phase-Change Technique to Thin Sections With Heating on Both Surfaces. NASA TN D-7193, 1973.

38. Bushnell, Dennis M.; and Weinstein, Leonard M.: Correlation of Peak Heating for Reattachment of Separated Flows. J. Spacecraft & Rockets, vol. 5, no. 9, Sept. 1968, pp. 1111-1112.

39. Sinha, Ram; Fox, Herbert; and Weinberger, Lawrence: An Implicit Finite Difference Solution for Jet and Wake Problems. Pt. II: Program Manual. ARL 70-0024, U.S. Air Force, Feb. 1970. (Available from DDC as AD 707 866.)

40. Oh, Y. H.: Analysis of Two-Dimensional Free Turbulent Mixing. AIAA Paper 74-594, June 1974.

TABLE I.- CENTER-LINE PROFILE DATA AT $p_o = 0.51$ MN/m^2 (5 atm) IN 11-INCH TUNNEL

(a) $T_o = 620$ K; $x = 3.30$ cm

y, cm	u, m/sec	M	$p_{t,2}$, N/m^2	p, N/m^2	$p_{t,1}$, N/m^2	T, K
0.0330	164.5	0.334	9 684	8963	9 684	603.2
.0330	168.9	.343	9 949	9170	9 949	602.5
.0330	190.8	.389	9 949	8963	9 949	598.6
.2622	251.1	.518	11 010	9170	11 010	585.3
.2861	262.1	.542	10 940	8963	10 940	582.5
.3291	241.6	.497	10 610	8963	10 610	587.6
.4150	266.5	.552	11 280	9170	11 280	581.3
.5869	258.2	.533	15 780	8963	15 578	583.5
.6633	266.5	.552	11 280	9170	11 280	581.3
.6633	265.9	.550	11 010	8963	11 010	581.5
.8018	449.5	.987	16 710	8963	16 710	516.1
.8162	574.0	1.346	26 270	9170	39 250	452.7
.8305	526.0	1.199	21 560	8963	31 490	478.9
.8376	589.3	1.396	27 190	8963	41 120	443.8
.8448	588.0	1.391	27 060	8963	28 180	444.5
.8544	649.5	1.607	35 150	9170	39 380	406.6
.8591	595.6	1.417	27 860	8963	42 360	440.0
.8752	645.6	1.592	33 830	8963	54 630	409.2
.8926	697.5	1.798	41 790	8963	51 370	374.5
.8973	737.3	1.978	50 670	9170	69 290	346.0
.9117	728.9	1.938	47 760	8963	63 690	352.2
.9164	744.3	2.011	51 070	8963	71 370	340.9
.9403	763.7	2.109	55 720	8963	83 180	326.3
.9546	786.3	2.232	63 280	9170	103 100	308.8
.9642	788.0	2.242	62 350	8963	102 400	303.3
.9881	793.4	2.273	63 940	8963	107 400	300.9
1.0263	796.4	2.290	64 870	8963	110 400	300.9
1.0454	792.0	2.265	65 000	9170	108 500	304.4
1.1456	796.4	2.290	64 870	8963	110 400	300.9

TABLE I.- Continued

(b) T_o = 623 K; x = 3.91 cm

y, cm	u m/sec	M	$p_{t,2}$, N/m^2	p, N/m^2	$p_{t,1}$, N/m^2	T, K
0.0330	144.2	0.292	9 949	9377	9 949	606.3
.2431	226.8	.466	10 880	9377	10 880	591.1
.2861	207.5	.424	10 610	9377	10 610	595.2
.2909	213.4	.437	10 610	9308	10 610	594.0
.3148	223.1	.458	10 750	9308	10 750	591.9
.4914	252.1	.520	11 280	9377	11 280	585.0
.5296	257.0	.531	11 280	9308	11 280	583.8
.5726	311.3	.651	12 470	9377	12 470	568.4
.6013	354.4	.751	13 530	9308	13 530	554.2
.6060	383.4	.821	14 590	9377	14 590	543.5
.6395	419.6	.910	15 920	9308	15 920	529.0
.6610	473.2	1.050	18 840	9377	18 840	505.2
.6681	479.6	1.068	19 230	9377	19 240	502.2
.6920	519.6	1.181	21 890	9308	22 010	482.2
.7206	577.3	1.357	27 190	9377	28 080	450.7
.7254	585.7	1.384	27 860	9308	28 950	445.9
.7589	648.6	1.604	35 820	9377	58 120	407.2
.7589	659.6	1.645	37 140	9308	42 310	400.1
.7923	674.9	1.705	39 530	9308	46 320	389.9
.7923	697.9	1.800	43 780	9377	53 860	374.2
.8209	729.6	1.941	49 750	9308	66 480	351.6
.8209	735.7	1.970	51 070	9308	69 490	347.2
.8376	741.6	1.998	52 800	9377	73 150	342.9
.8400	739.9	1.990	52 400	9377	72 210	344.2
.8639	756.9	2.074	56 110	9308	81 780	331.4
.8687	760.0	2.090	57 310	9377	84 420	329.1
.8878	772.0	2.153	60 090	9308	92 520	320.0
.9594	783.6	2.217	63 410	9308	102 200	311.0
1.0048	785.1	2.220	64 340	9377	104 400	309.8
1.0836	782.7	2.212	63 140	9308	101 500	311.7
1.1695	784.0	2.219	64 010	9377	103 300	310.7
1.2125	782.3	2.209	63 010	9308	101 000	312.0

TABLE I.- Continued

(c) T_o = 619 K; x = 4.57 cm

y, cm	u, m/sec	M	$p_{t,2}$, N/m^2	p, N/m^2	$p_{t,1}$, N/m^2	T, K
0.0330	61.6	0.124	9 617	9515	9 617	614.8
.0330	93.6	.189	9 684	9446	9 684	612.3
.0330	116.4	.235	9 816	9446	9 816	609.9
.0330	125.3	.253	9 949	9515	9 949	608.9
.1858	201.3	.411	10 610	9446	10 610	596.5
.2431	215.6	.442	10 880	9515	10 880	593.5
.2766	215.6	.442	10 880	9515	10 880	593.5
.3052	221.3	.454	10 880	9446	10 880	592.3
.3577	242.2	.499	11 280	9515	11 280	587.5
.4150	283.2	.588	11 940	9446	11 940	576.7
.4771	335.0	.706	13 270	9515	13 270	560.8
.5440	487.6	1.090	19 900	9446	19 910	498.3
.5726	504.5	1.137	21 220	9515	21 280	490.0
.6013	579.2	1.363	27 590	9446	28 540	449.6
.6347	620.0	1.500	32 240	9446	34 670	425.3
.6586	626.4	1.523	33 300	9515	36 100	421.3
.6633	614.6	1.481	31 570	9446	33 740	428.6
.6872	684.9	1.746	41 790	9446	49 960	383.2
.6968	692.4	1.777	43 110	9446	52 390	378.0
.7254	715.4	1.876	47 490	9446	61 020	361.9
.7302	700.8	1.812	44 970	9515	55 710	372.2
.7302	721.9	1.905	48 820	9446	63 830	357.3
.7350	704.3	1.827	45 630	9515	57 010	369.7
.7780	752.1	2.050	55 720	9446	79 860	335.1
.7827	745.0	2.015	54 390	9515	76 180	340.1
.7971	752.0	2.050	56 110	9515	80 420	335.1
.8066	752.1	2.050	55 720	9446	79 860	335.1
.8162	761.3	2.097	58 500	9515	86 580	328.1
.8448	773.6	2.162	61 420	9446	95 130	318.8
.8687	773.9	2.163	61 950	9515	96 050	318.5
.9499	778.4	2.188	63 280	9515	99 880	315.0
.9594	777.7	2.184	62 610	9446	98 560	315.5
.9713	773.4	2.161	61 820	9515	95 680	318.9
1.0167	775.4	2.172	61 950	9446	96 640	317.3
1.1624	773.4	2.161	61 820	9515	95 680	318.9

TABLE I.- Continued

(d) T_o = 611 K; x = 5.21 cm

y, cm	u, m/sec	M	$p_{t,2}$, N/m^2	p, N/m^2	$p_{t,1}$, N/m^2	T, K
0.1237	103.2	0.208	9 949	9653	9 949	611.4
.1763	181.9	.370	10 610		10 610	600.2
.3004	208.9	.427	10 940		10 940	594.9
.3339	255.9	.528	11 670		11 670	584.1
.3864	323.0	.678	13 130		13 130	564.7
.3959	301.4	.629	12 600		12 600	571.4
.4914	470.7	1.043	19 230		19 230	506.4
.4962	447.8	.983	17 910		17 910	516.8
.4962	459.6	1.014	18 570		18 570	511.5
.5726	551.7	1.276	25 470		37 570	465.1
.5869	578.5	1.361	28 120		29 070	450.0
.6251	620.7	1.502	33 030		35 550	424.9
.6347	616.5	1.488	32 500		34 810	427.4
.6347	641.3	1.577	35 820		39 630	411.9
.6633	655.8	1.631	37 940		42 940	402.6
.6681	660.1	1.647	38 600		44 010	399.7
.6920	672.5	1.696	40 590		47 340	391.5
.6920	688.7	1.761	43 380		52 280	380.6
.7111	693.1	1.780	44 170		53 760	377.5
.7206	709.0	1.848	47 230		59 690	366.4
.7732	736.1	1.972	53 060		72 290	346.9
.7732	740.1	1.991	53 990		74 450	344.0
.8185	750.9	2.044	56 640		80 880	336.0
.8400	756.6	2.073	58 100		84 580	331.7
.9833	759.1	2.086	58 770		86 310	329.8
1.0454	761.1	2.096	59 300		87 770	328.3
1.2006	758.9	2.084	58 700		86 130	330.0
1.3223	760.6	2.093	59 160		87 350	328.6

TABLE I.- Concluded

(e) T_o = 618 K; x = 5.84 cm

y, cm	u, m/sec	M	$p_{t,2}$, N/m^2	p, N/m^2	$p_{t,1}$, N/m^2	T, K
0.0330	33.7	0.068	9 684	9653	9 684	616.1
.0330	36.7	.073	9 551	9515	9 551	616.0
.0330	62.6	.126	9 551	9446	9 551	614.7
.0330	77.0	.155	9 816	9653	9 816	613.7
.1237	181.9	.370	10 610	9653	10 610	600.2
.1524	178.4	.363	10 350	9446	10 350	600.8
.1620	181.9	.370	10 610	9653	10 610	600.2
.2527	301.4	.629	12 600	9653	12 600	571.4
.2718	325.1	.683	13 000	9515	13 000	564.1
.2813	346.7	.733	13 800	9653	13 800	556.8
.2861	360.7	.766	13 930	9446	13 930	551.9
.3577	445.3	.976	17 780	9653	17 780	517.9
.4198	524.4	1.194	23 080	9653	23 240	479.8
.4294	522.8	1.190	22 950	9653	23 090	480.6
.4485	532.1	1.217	23 210	9446	23 420	475.7
.4723	579.8	1.365	27 860	9515	28 820	449.3
.4819	565.6	1.319	26 800	9653	27 460	457.4
.5010	601.2	1.435	30 640	9653	32 290	436.7
.5392	623.8	1.513	33 430	9653	36 120	423.0
.5440	642.1	1.579	35 150	9446	38 940	411.4
.5583	644.1	1.587	36 210	9653	40 240	410.1
.5869	668.5	1.680	39 930	9653	46 210	394.2
.6299	704.6	1.829	45 370	9446	56 730	369.5
.6395	705.0	1.830	46 430	9653	58 100	369.3
.6490	709.1	1.848	46 560	9515	58 860	366.4
.7063	730.3	1.944	51 740	9653	69 270	351.2
.7302	743.9	2.009	54 120	9515	75 540	341.2
.7326	736.1	1.972	53 060	9653	72 290	346.9
.7923	747.7	2.028	55 850	9653	78 910	338.3
.8018	755.7	2.068	57 040	9515	82 780	332.4
.8782	754.7	2.063	56 380	9446	81 540	333.1
1.0215	753.7	2.058	56 110	9446	80 870	333.9
1.0645	756.7	2.073	57 310	9515	83 460	331.6
1.1361	753.7	2.058	56 110	9446	80 870	333.9

TABLE II.- CENTER-LINE PROFILE DATA AT p_0 = 1.014 MN/m^2 (10 atm) IN 11-INCH TUNNEL

(a) T_0 = 619 K; x = 3.30 cm

y, cm	u, m/sec	M	$p_{t,2}$, N/m^2	p, N/m^2	$p_{t,1}$, N/m^2	T, K
0.033	289.0	0.601	18 570	14 550	18 570	574.9
.033	271.8	.563	18 040	14 550	18 040	579.7
.033	267.1	.553	17 910	14 550	17 910	581.0
.033	259.5	.536	17 780	14 620	17 780	583.0
.033	264.2	.547	17 910	14 620	17 910	581.7
.038	267.1	.553	17 910	14 550	17 910	581.0
.322	270.8	.561	18 440	14 890	18 440	580.0
.399	238.7	.491	17 640	14 960	17 640	588.1
.550	272.3	.564	18 570	14 960	18 570	579.6
.650	272.4	.564	18 570	14 960	18 570	579.5
.658	272.3	.564	18 570	14 960	18 570	579.6
.661	267.9	.555	18 440	14 960	18 440	580.7
.679	263.3	.545	18 310	14 960	18 310	582.0
.717	269.5	.558	18 570	15 030	18 570	580.3
.793	308.8	.646	19 900	15 030	19 900	569.0
.795	322.4	.677	20 430	15 030	20 430	564.7
.814	355.1	.753	21 890	15 030	21 890	553.7
.816	368.2	.784	22 550	15 030	22 550	549.0
.835	421.8	.916	25 870	15 030	25 870	527.9
.867	510.4	1.154	34 220	15 030	34 350	486.8
.890	574.3	1.347	43 120	15 030	44 430	452.3
.924	631.1	1.540	53 590	15 030	58 460	418.2
.938	596.2	1.419	46 830	15 030	49 120	439.5
.945	667.5	1.676	61 950	15 030	71 580	394.7
.976	732.3	1.954	80 920	14 960	10 900	349.5
.984	735.0	1.967	82 250	15 030	11 170	347.6
1.006	755.2	2.066	89 940	15 030	13 030	332.6
1.023	777.7	2.185	99 230	14 960	15 630	315.4
1.029	773.9	2.164	97 500	14 960	15 130	318.3
1.040	782.8	2.213	101 600	14 960	16 330	311.4
1.046	786.7	2.235	103 500	14 960	16 900	308.4
1.055	788.3	2.244	104 300	14 960	17 150	307.1
1.087	793.0	2.271	106 100	14 890	17 850	303.4
1.151	797.4	2.297	107 800	14 820	18 450	300.0
1.220	794.5	2.280	106 400	14 820	17 970	302.2

TABLE II.- Continued

(b) T_o = 613 K; x = 3.91 cm

y, cm	u, m/sec	M	$p_{t,2}$, N/m^2	p, N/m^2	$p_{t,1}$, N/m^2	T, K
0.033	172.8	0.351	15 920	14 620	15 920	601.6
.033	239.0	.492	17 240	14 620	17 240	588.0
.033	188.3	.384	16 180	14 620	16 180	598.8
.231	277.7	.576	18 310	14 620	18 310	578.1
.235	239.0	.492	17 240	14 620	17 240	588.0
.270	244.3	.503	17 370	14 620	17 370	586.8
.428	259.4	.536	17 770	14 620	17 770	583.0
.501	259.4	.536	17 770	14 620	17 770	583.0
.531	286.3	.595	18 570	14 620	18 570	575.7
.627	319.9	.671	19 770	14 620	19 770	565.5
.649	305.7	.639	19 240	14 620	19 240	570.0
.675	379.9	.812	22 550	14 620	22 550	544.6
.725	496.2	1.114	31 700	14 620	31 750	493.9
.747	555.6	1.289	39 130	14 620	39 880	462.8
.753	546.2	1.260	37 800	14 620	38 350	468.0
.755	523.8	1.193	34 890	14 620	35 120	479.9
.760	575.9	1.352	42 180	14 620	43 520	451.4
.772	569.1	1.331	41 120	14 620	42 230	455.3
.792	627.9	1.528	51 470	14 620	55 910	420.2
.811	635.7	1.556	53 060	14 620	58 250	415.3
.819	645.0	1.590	55 050	14 620	61 260	409.4
.866	710.4	1.855	71 640	14 550	90 890	365.2
.889	739.4	1.988	81 190	14 550	111 800	344.3
.912	764.3	2.113	91 130	14 620	136 400	325.7
.977	784.7	2.224	100 200	14 620	162 200	309.9
1.029	792.6	2.269	103 500	14 550	173 300	303.7
1.172	791.3	2.261	102 800	14 550	171 200	304.8

TABLE II.- Continued

(c) T_0 = 616 K; x = 4.57 cm

y, cm	u, m/sec	M	$p_{t,2}$, N/m^2	p, N/m^2	$p_{t,1}$, N/m^2	T, K
0.033	189.1	0.386	17 110	15 440	17 110	598.7
.033	174.1	.354	16 840	15 440	16 840	601.4
.033	195.9	.400	17 240	15 440	17 240	597.4
.056	195.9	.400	17 240	15 440	17 240	597.4
.111	223.0	.457	17 910	15 510	17 910	591.7
.142	223.0	.457	17 910	15 510	17 910	591.7
.211	234.0	.481	18 170	15 510	18 170	589.2
.231	228.7	.470	18 040	15 510	18 040	590.4
.323	234.0	.481	18 170	15 510	18 170	589.2
.326	234.0	.481	18 170	15 510	18 170	589.2
.500	271.7	.563	19 240	15 510	19 240	579.7
.550	356.3	.756	22 550	15 440	22 550	553.3
.589	447.7	.983	28 520	15 380	28 520	516.7
.601	488.6	1.093	32 500	15 380	32 530	497.7
.610	463.8	1.025	29 980	15 380	29 980	509.4
.638	533.4	1.221	37 800	15 310	38 160	474.9
.642	532.1	1.217	37 800	15 380	38 150	475.5
.647	528.4	1.207	37 140	15 310	37 440	477.5
.678	594.1	1.412	47 090	15 240	49 300	440.8
.684	582.7	1.372	45 110	15 240	46 770	447.5
.700	623.7	1.513	52 530	15 170	56 760	422.8
.715	648.1	1.602	57 840	15 170	64 670	407.4
.725	664.2	1.663	61 690	15 170	70 850	396.9
.729	665.8	1.670	61 820	15 100	71 210	395.8
.750	700.5	1.811	70 970	15 030	87 870	372.2
.767	726.7	1.928	78 270	14 820	103 800	353.6
.775	726.7	1.928	78 270	14 820	103 800	353.6
.785	737.4	1.978	81 590	14 750	111 600	345.8
.787	748.5	2.032	85 690	14 750	121 400	337.6
.803	764.1	2.112	91 930	14 750	137 500	325.8
.806	751.6	2.048	86 890	14 750	124 400	335.3
.813	767.9	2.132	93 520	14 750	141 800	322.9
.821	779.1	2.193	98 030	14 690	155 200	314.3
.828	777.1	2.187	97 110	14 690	152 500	315.9
.831	768.9	2.137	93 520	14 690	142 400	322.2
.858	792.0	2.265	104 100	14 690	173 900	304.2
.862	783.4	2.217	100 000	14 690	161 200	310.9
.864	793.0	2.271	104 100	14 620	174 700	303.5
.875	796.1	2.290	105 700	14 620	179 800	300.9
.895	794.3	2.279	104 800	14 620	176 800	302.4
.895	799.5	2.310	107 400	14 620	185 600	298.3
.898	793.0	2.271	104 100	14 620	174 700	303.5
.926	797.2	2.296	106 800	14 690	182 500	300.1
.936	797.6	2.298	107 400	14 750	183 900	299.8
1.018	796.6	2.292	107 400	14 820	183 100	300.6
1.085	794.0	2.277	106 100	14 820	178 800	302.6

TABLE II.- Concluded

(d) T_o = 621 K; x = 5.21 cm

y, cm	u, m/sec	M	$p_{t,2}$ N/m^2	p, N/m^2	$p_{t,1}$, N/m^2	T, K
0.033	65.3	0.132	16 050	15 860	16 050	614.4
.033	125.3	.253	16 580	15 860	16 580	608.7
.156	190.1	.388	17 510	15 790	17 510	598.5
.211	179.7	.366	17 240	15 720	17 240	600.4
.303	216.1	.443	17 910	15 650	17 910	593.2
.403	228.7	.470	18 040	15 510	18 040	590.4
.417	239.2	.492	18 310	15 510	18 310	588.0
.477	289.1	.602	19 640	15 380	19 640	574.9
.568	447.5	.982	28 250	15 240	28 250	516.8
.577	436.2	.953	27 320	15 240	27 320	521.7
.586	453.7	.998	28 790	15 240	28 790	514.0
.591	478.7	1.065	31 170	15 240	31 180	502.4
.609	515.4	1.168	35 150	15 170	35 310	484.3
.646	565.1	1.318	42 050	15 170	43 080	457.5
.659	565.1	1.318	42 050	15 170	43 080	457.5
.673	593.0	1.408	46 690	15 170	48 830	441.4
.696	626.2	1.522	53 060	15 170	57 520	421.2
.714	652.7	1.619	85 430	15 170	66 330	404.4
.723	646.9	1.598	57 570	15 170	64 250	408.1
.737	670.4	1.688	63 270	15 170	73 510	392.7
.838	751.5	2.047	88 880	15 100	127 200	335.3
.856	762.2	2.102	93 260	15 100	138 500	327.3
.883	771.9	2.154	97 500	15 100	150 100	319.8
.947	779.5	2.195	101 000	15 100	160 100	314.0
.993	783.0	2.214	102 100	15 030	164 300	311.3
1.021	782.6	2.212	101 500	14 960	162 900	311.6
1.153	786.5	2.234	101 500	14 960	165 600	308.5

TABLE III.- OFF-CENTER-LINE PROFILE DATA AT p_o = 1.014 MN/m^2 (10 atm) IN 11-INCH TUNNEL

(a) Profile data 1.27 cm to the right of the center line. T_o = 617 K; x = 5.21 cm

y, cm	u, m/sec	M	$p_{t,2}$, N/m^2	p, N/m^2	$p_{t,1}$, N/m^2	T, K
0.1830	130.3	0.264	16 380	15 600	16 380	608.2
.1830	142.7	.289	16 890	15 940	16 890	606.5
.1830	154.5	.314	17 060	15 940	17 060	604.8
.2546	195.4	.399	17 410	15 600	17 410	597.7
.3359	231.7	.476	18 620	15 940	18 620	589.9
.3453	238.4	.490	18 790	15 940	18 790	588.4
.3837	264.8	.548	19 130	15 600	19 130	581.8
.3931	278.7	.578	19 990	15 940	19 990	578.0
.4360	342.5	.723	22 580	15 940	22 580	558.3
.4505	356.2	.755	23 270	15 940	23 270	553.5
.4695	392.3	.842	24 820	15 600	24 820	540.1
.4792	407.4	.879	26 370	15 940	26 370	534.0
.4982	421.5	.915	27 410	15 940	27 410	528.2
.5076	448.6	.985	29 650	15 940	29 650	516.5
.5173	451.8	.993	29 300	15 600	29 300	515.0
.5602	510.3	1.154	35 510	15 600	35 630	487.0
.5699	522.9	1.190	37 920	15 940	38 160	480.5
.6318	612.8	1.475	52 920	15 940	56 440	429.7
.6796	677.6	1.716	68 430	15 940	80 590	388.1
.6796	669.5	1.684	64 810	15 600	75 150	393.5
.6844	673.2	1.698	67 220	15 940	78 500	391.1
.7083	705.6	1.833	76 880	15 940	96 350	368.8
.7131	704.2	1.827	74 810	15 600	93 440	369.8
.7418	727.6	1.932	84 460	15 940	112 200	353.1
.7512	733.9	1.961	84 940	15 600	115 000	348.5
.7560	747.3	2.026	92 050	15 940	129 900	338.7
.7703	747.3	2.026	90 110	15 600	127 200	338.6
.8086	770.2	2.143	102 000	15 940	156 000	321.4
.8277	774.4	2.166	101 800	15 600	158 200	318.1
.8325	780.2	2.198	106 900	15 940	169 900	313.7
.8706	782.0	2.208	107 800	15 940	172 500	312.3
.8754	784.8	2.223	106 900	15 600	173 100	310.1
.8851	787.0	2.236	101 300	15 940	180 300	308.4
.9948	787.9	2.241	101 800	15 940	181 800	307.6

TABLE III.- Concluded

(b) Profile data 1.27 cm to the left of the center line.
T_o = 617 K; x = 5.21 cm

y, cm	u, m/sec	M	$p_{t,2}$, N/m^2	p, N/m^2	$p_{t,1}$, N/m^2	T, K
0.1830	196.0	0.400	17 240	15 440	17 240	597.5
.1830	175.5	.357	17 410	15 940	17 410	601.3
.1830	184.9	.377	17 580	15 940	17 580	599.6
.2546	227.6	.467	17 930	15 440	17 930	590.9
.3359	250.9	.517	19 130	15 940	19 130	585.3
.3453	244.8	.504	18 960	15 940	18 960	586.8
.3837	301.8	.630	20 170	15 440	20 170	571.3
.3931	298.1	.622	20 680	15 940	20 680	572.4
.4360	359.5	.763	23 440	15 940	23 440	552.3
.4505	369.0	.786	23 960	15 940	23 960	548.9
.4695	416.8	.903	26 200	15 440	26 200	530.2
.4792	426.0	.926	27 750	15 940	27 750	526.3
.4982	432.5	.943	28 270	15 940	28 270	523.6
.5076	466.8	1.033	31 370	15 940	31 370	508.2
.5173	475.0	1.055	31 200	15 440	31 200	504.3
.5602	531.9	1.217	37 920	15 440	38 260	475.8
.5699	534.2	1.223	39 470	15 940	39 860	474.6
.6318	628.3	1.529	56 190	15 940	61 060	420.1
.6796	690.5	1.769	72 190	15 940	87 360	379.3
.6796	687.7	1.757	69 090	15 440	83 090	381.2
.6844	685.4	1.748	70 670	15 940	84 580	382.8
.7083	718.3	1.889	81 150	15 940	105 100	359.8
.7131	721.4	1.903	79 630	15 440	104 000	357.6
.7418	739.5	1.988	88 940	15 940	122 400	344.4
.7512	749.4	2.036	89 980	15 440	127 800	337.1
.7560	758.2	2.081	96 660	15 940	141 500	330.4
.7703	761.4	2.097	94 940	15 440	140 500	328.1
.8086	776.2	2.176	104 900	15 940	164 200	316.7
.8277	783.8	2.218	105 300	15 440	169 900	310.8
.8325	785.6	2.228	109 600	15 940	178 200	309.4
.8706	787.0	2.236	101 300	15 940	180 300	308.4
.8754	791.7	2.263	109 300	15 440	182 300	304.6
.8851	785.6	2.228	109 600	15 940	178 200	309.4
.9948	791.8	2.264	112 900	15 940	188 300	304.6

TABLE IV.- CENTER-LINE PROFILE DATA AT NOMINAL p_o = 10 atm

IN 20-INCH TUNNEL

(a) T_o = 463 K; p_o = 1.014 MN/m^2 (10 atm); x = 3.43 cm

y, cm	u, m/sec	M	$p_{t,2}$, N/m^2	p, N/m^2	$p_{t,1}$, N/m^2	T, K
0.023	216.8	0.517	30 200	25 170	30 200	438.1
.329	228.4	.547	30 460	24 860	30 460	434.2
.349	228.8	.549	30 200	24 610	30 200	433.1
.351	229.8	.549	31 110	25 340	31 110	435.7
.391	233.2	.558	30 720	24 860	30 720	434.0
.430	234.6	.562	30 070	24 270	30 070	433.8
.470	233.7	.559	31 620	25 580	31 620	435.3
.524	234.3	.560	30 070	24 300	30 070	435.9
.547	239.8	.574	30 460	24 370	30 460	435.0
.601	280.5	.679	32 790	24 080	32 790	424.8
.656	378.5	.954	43 800	24 390	43 800	391.9
.726	516.8	1.417	74 650	23 990	78 270	330.8
.790	627.3	1.905	126 300	24 400	165 000	269.9
.821	657.0	2.082	152 100	25 060	222 900	247.9
.899	673.2	2.187	164 300	24 750	259 100	235.9
.930	674.0	2.187	161 800	24 350	255 200	236.4

TABLE IV.- Continued

(b) T_0 = 455 K; p_0 = 1.02 MN/m^2 (10 atm); x = 3.89 cm

y, cm	u, m/sec	M	$p_{t,2}$, N/m^2	p, N/m^2	$p_{t,1}$, N/m^2	T, K
0.033	199.3	0.477	30 200	25 850	30 200	435.2
.318	215.9	.518	31 110	25 900	31 110	431.9
.318	215.5	.518	30 850	25 700	30 850	431.3
.507	290.7	.714	35 510	25 280	35 510	412.4
.566	385.6	.986	48 340	25 950	48 340	380.5
.630	491.5	1.341	73 110	25 680	75 230	334.6
.661	539.2	1.526	89 060	25 350	96 670	310.7
.690	585.3	1.730	108 800	24 970	129 000	284.8
.702	599.4	1.794	116 100	25 000	142 400	277.8
.726	621.0	1.901	130 200	25 310	169 800	265.7
.769	647.4	2.052	149 300	25 250	214 400	247.7
.811	659.7	2.124	160 900	25 560	242 600	240.2
.845	661.9	2.138	160 400	25 170	244 200	238.6
.947	661.1	2.127	160 400	25 400	242 400	240.4
1.164	665.3	2.153	165 400	25 620	254 600	237.7

TABLE IV.- Continued

(c) T_o = 458 K; p_o = 1.02 MN/m^2 (10 atm); x = 4.62 cm

y, cm	u, m/sec	M	$p_{t,2}$, N/m^2	p, N/m^2	$p_{t,1}$, N/m^2	T, K
0.101	184.7	0.437	30 330	26 590	30 330	443.8
.159	189.3	.449	29 810	25 950	29 810	440.8
.226	194.3	.462	30 200	26 080	30 200	439.9
.251	198.9	.474	31 360	26 900	31 360	439.0
.285	199.4	.475	31 110	26 650	31 110	438.7
.301	201.7	.480	30 850	26 340	30 850	439.1
.328	209.6	.500	30 980	26 110	30 980	437.3
.359	223.3	.535	31 490	25 920	31 490	434.2
.378	238.8	.574	32 140	25 710	32 140	431.0
.437	302.4	.742	36 810	25 530	36 810	413.4
.460	338.3	.841	40 170	25 270	40 170	402.3
.476	362.9	.912	42 890	25 040	42 890	394.5
.530	431.1	1.122	58 830	26 870	58 940	367.7
.593	521.9	1.449	86 360	26 790	91 370	322.9
.623	558.0	1.598	100 300	26 410	111 900	303.6
.664	598.0	1.780	119 200	26 020	145 100	208.8
.696	626.7	1.925	135 300	25 690	179 000	263.8
.720	638.4	1.989	147 000	26 320	202 500	256.4
.751	648.4	2.048	154 400	26 230	221 000	249.6
.837	654.4	2.085	158 200	26 000	232 100	245.3
.857	654.5	2.083	157 900	25 990	231 500	245.7
.892	653.7	2.080	158 900	26 230	232 500	245.9
.983	653.6	2.078	157 800	26 100	230 500	246.3
1.035	654.1	2.081	154 700	25 520	226 400	246.1

TABLE IV.- Concluded

(d) T_o = 456 K; p_o = 1.05 MN/m^2 (10 atm); x = 5.31 cm

y, cm	u, m/sec	M	$p_{t,2}$ N/m^2	p, N/m^2	$p_{t,1}$ N/m^2	T, K
0.091	173.2	0.411	30 590	27 240	30 590	443.2
.134	176.4	.418	30 070	26 660	30 070	442.8
.229	199.3	.474	33 570	28 780	33 570	440.2
.275	237.9	.573	34 470	27 600	34 470	429.2
.343	321.0	.795	40 820	26 920	40 820	406.0
.408	404.8	1.042	52 610	26 450	52 620	375.8
.468	477.1	1.281	71 560	26 960	72 840	345.0
.502	518.6	1.438	87 520	27 490	92 300	323.8
.503	521.6	1.452	87 650	27 110	92 810	321.5
.534	556.4	1.596	100 900	26 620	112 500	302.4
.549	569.6	1.654	107 500	26 690	122 900	295.3
.604	613.8	1.868	132 000	26 460	168 900	268.6
.648	635.7	1.978	152 500	27 590	208 600	257.1
.682	646.3	2.040	159 800	27 340	227 600	249.9
.722	651.9	2.071	162 900	27 100	237 000	246.6
.819	653.3	2.079	162 200	26 790	237 100	245.8
.882	653.4	2.079	160 100	26 460	234 000	245.9

TABLE V.- CENTER-LINE PROFILE DATA AT NOMINAL p_o = 35 atm IN 20-INCH TUNNEL

(a) T_o = 478 K; p_o = 3.49 MN/m^2 (35 atm); x = 4.19 cm

y, cm	u, m/sec	M	$p_{t,2}$, N/m^2	p, N/m^2	$p_{t,1}$, N/m^2	T, K
0.213	209.2	0.491	99 620	84 490	99 620	452.2
.520	234.7	.552	101 700	82 660	101 700	450.1
.686	254.8	.603	104 800	81 930	104 800	444.1
.720	285.7	.682	111 700	81 850	111 700	437.1
.745	314.0	.756	119 400	81 740	119 400	429.0
.766	352.4	.861	132 600	81 740	132 600	417.4
.795	402.8	1.007	156 000	81 760	156 000	398.6
.832	456.6	1.177	191 400	81 710	192 400	374.4
.931	559.2	1.555	296 500	81 810	325 300	322.0
.940	622.7	1.840	397 400	81 830	500 200	284.9
.959	641.6	1.937	435 500	81 800	580 500	273.0
1.015	674.8	2.122	514 200	81 780	774 600	251.6
1.074	681.7	2.165	533 200	81 730	828 000	246.7
1.224	682.7	2.172	536 300	81 780	836 500	246.0

TABLE V.- Continued

(b) T_o = 500 K; p_o = 3.44 MN/m^2 (35 atm); x = 4.93 cm

y, cm	u, m/sec	M	$p_{t,2}$, N/m^2	p, N/m^2	$p_{t,1}$, N/m^2	T, K
0.027	198.1	0.451	98 330	85 530	98 330	480.5
.080	209.1	.478	100 100	85 650	100 100	476.8
.158	213.0	.487	99 620	84 720	99 620	476.9
.221	216.1	.494	98 330	83 230	98 330	476.7
.285	219.1	.501	97 560	82 210	97 560	476.8
.502	243.6	.560	102 700	82 990	102 700	470.4
.528	264.0	.610	106 000	82 470	106 000	465.9
.559	312.4	.734	117 400	82 070	117 400	451.5
.560	312.6	.734	117 400	82 060	117 400	451.8
.598	366.8	.880	135 900	82 080	135 900	432.3
.634	432.0	1.069	169 700	82 610	169 800	406.4
.676	503.7	1.299	224 800	82 990	229 500	374.6
.676	508.5	1.315	229 300	83 050	234 800	372.4
.724	589.1	1.622	323 500	83 100	364 700	328.5
.787	660.1	1.951	448 200	83 120	602 600	285.0
.832	684.8	2.083	505 000	83 140	740 400	269.0
.849	687.5	2.109	514 500	82 790	768 100	264.5
.850	688.1	2.110	515 600	82 880	770 200	264.6
.874	691.0	2.129	522 100	82 610	790 000	262.3
.993	691.6	2.133	522 400	82 360	792 700	261.7
.994	691.6	2.133	523 000	82 460	793 700	261.7
1.055	691.4	2.130	519 600	82 120	786 700	262.3

TABLE V.- Concluded

(c) T_o = 497 K; p_o = 3.44 MN/m^2 (35 atm); x = 5.61

y, cm	u, m/sec	M	$p_{t,2}$, N/m^2	p, N/m^2	$p_{t,1}$, N/m^2	T, K
0.027	177.6	0.402	97 560	87 280	97 560	486.2
.087	196.7	.447	88 330	85 370	88 330	482.0
.151	202.0	.460	97 810	84 590	97 810	479.3
.152	200.5	.455	98 590	85 530	98 590	482.9
.264	215.7	.495	100 900	85 370	100 900	473.6
.265	214.4	.490	99 100	84 080	99 100	475.7
.380	282.9	.661	116 500	86 910	116 500	456.7
.474	418.8	1.034	169 200	85 940	169 200	408.7
.527	512.0	1.335	241 400	85 340	248 200	366.0
.616	613.1	1.739	374 200	85 180	445 700	309.6
.656	651.0	1.922	446 900	85 160	590 200	285.6
.668	660.1	1.968	466 200	85 120	633 500	280.1
.696	675.9	2.053	502 700	84 960	722 400	269.7
.748	686.7	2.113	530 200	85 020	793 600	262.9
.782	689.2	2.127	539 000	85 380	814 700	261.3
.818	690.4	2.135	547 200	86 110	831 500	260.3
.920	690.0	2.134	547 200	86 190	830 900	260.3
.985	688.9	2.131	546 700	86 340	828 300	260.2
1.072	687.9	2.124	544 500	86 470	821 400	261.0

TABLE VI.- SUMMARY OF EXPERIMENTAL RESULTS

M_2	$N_{Re,T}$	u_3/u_2	λ	$N_{Re,T,0}$	Tunnel	$M_{\Delta V}$
1.79	3.0×10^4	0.360	0.470	1.41×10^4	11 inch	1.15
1.99	6.1	.270	.574	3.50	20 inch	1.45
2.06	5.7	.289	.552	3.20	20 inch	1.46
2.17	5.2	.256	.592	3.10	20 inch	1.61
2.22	5.6	.259	.589	3.30	20 inch	1.65
2.22	6.5	.259	.589	3.80	20 inch	1.65
2.30	4.3	.310	.527	2.50	11 inch	1.60

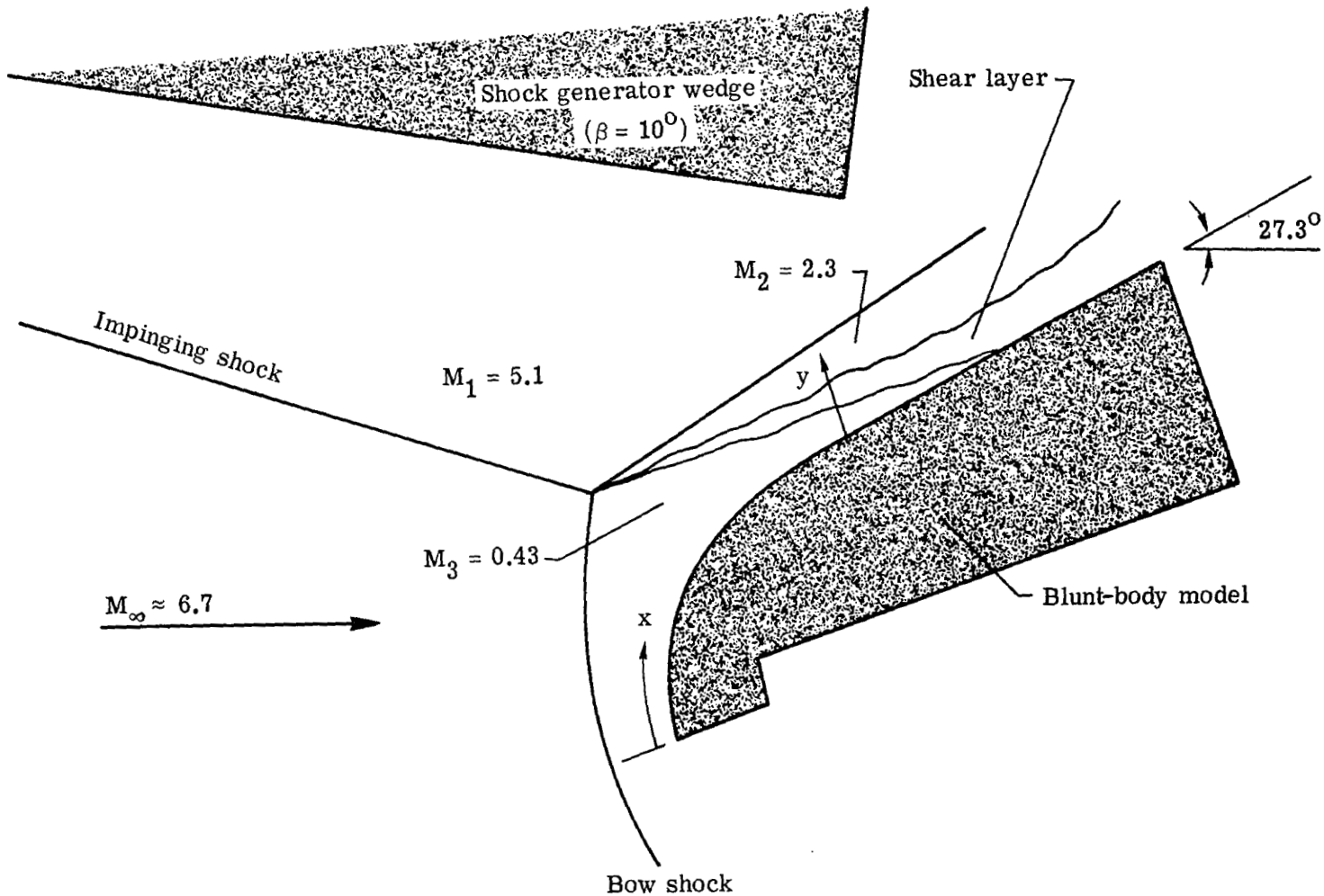

(a) Flow field for 11-inch tunnel tests.

Figure 1.- Sketches of flow fields.

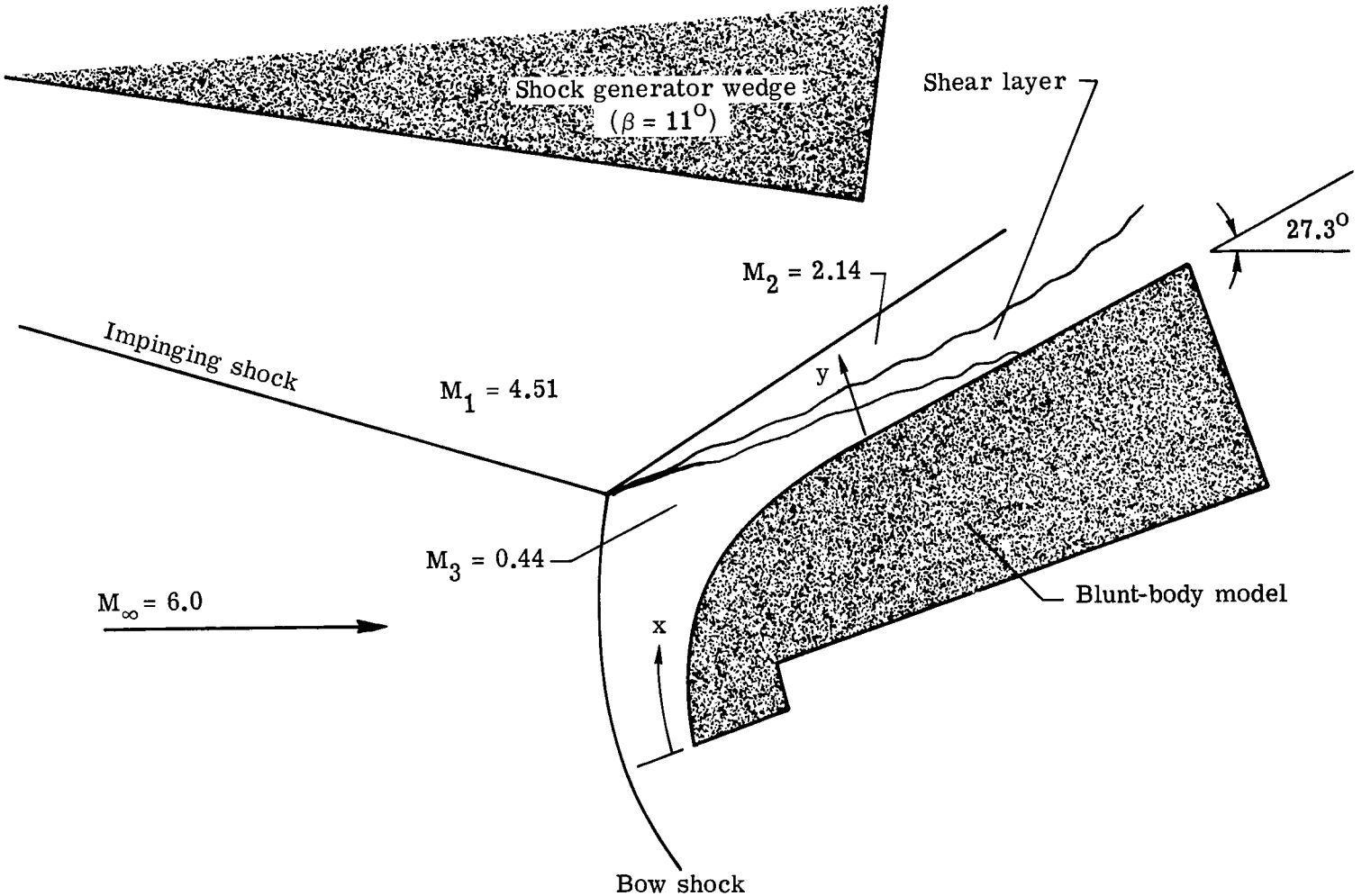

(b) Flow field for 20-inch tunnel tests.

Figure 1.- Concluded.

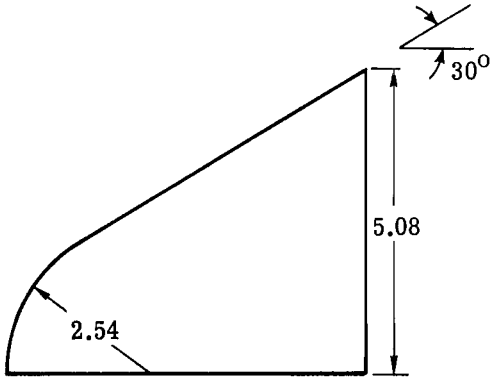

Blunt-body model

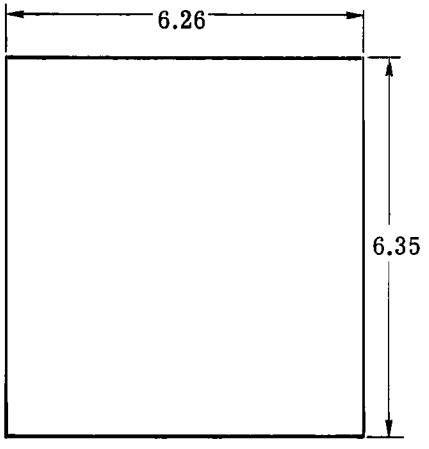

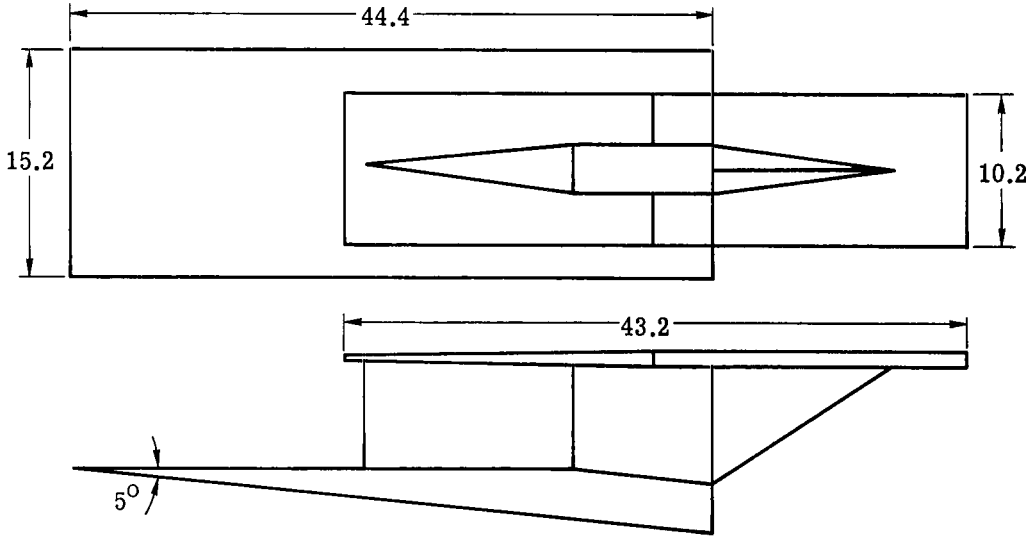

Shock generator wedge

Figure 2.- First set of models. All dimensions are in cm.

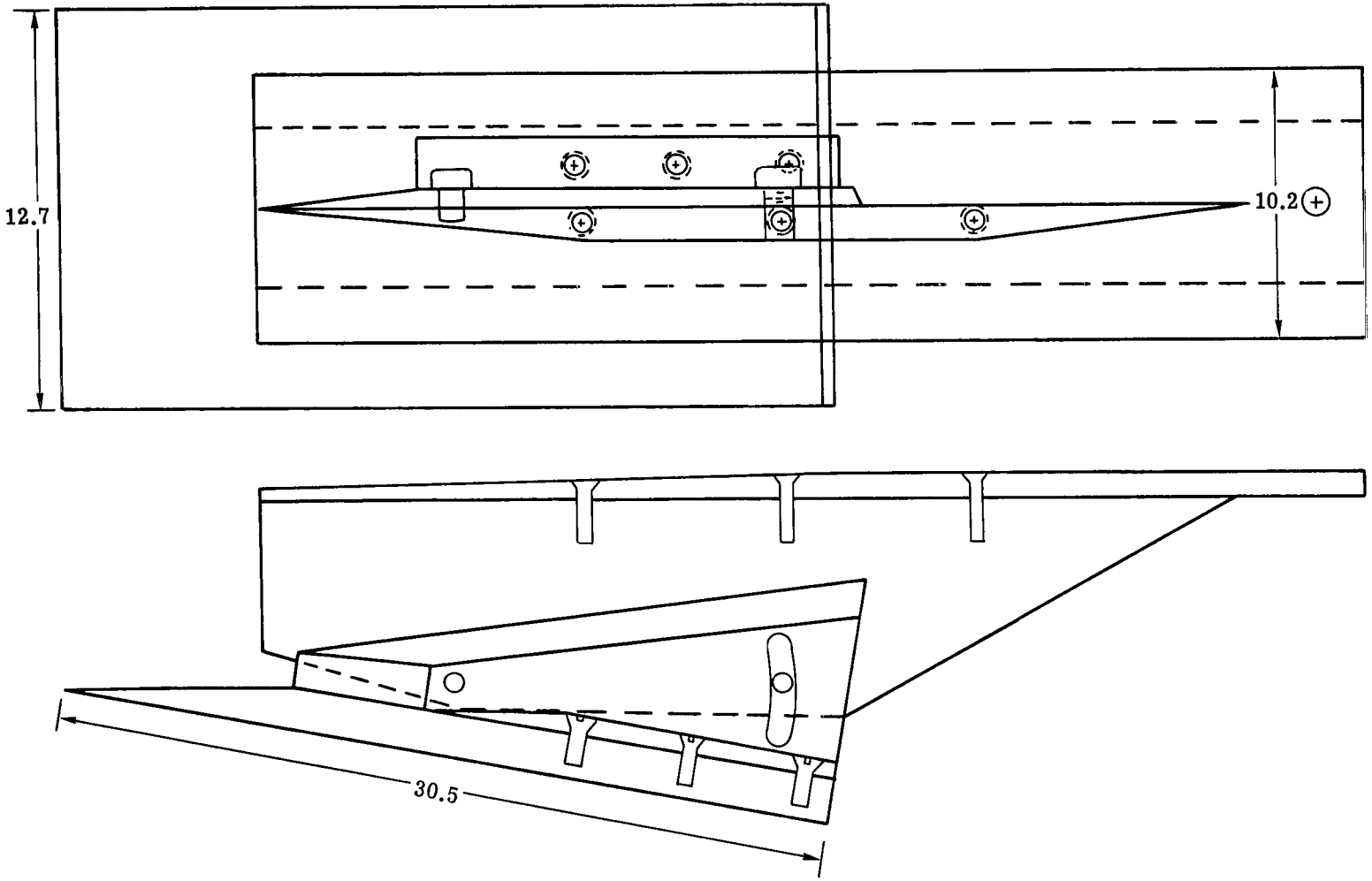

(a) Shock generator wedge.

Figure 3.- Second set of models. All dimensions are in cm.

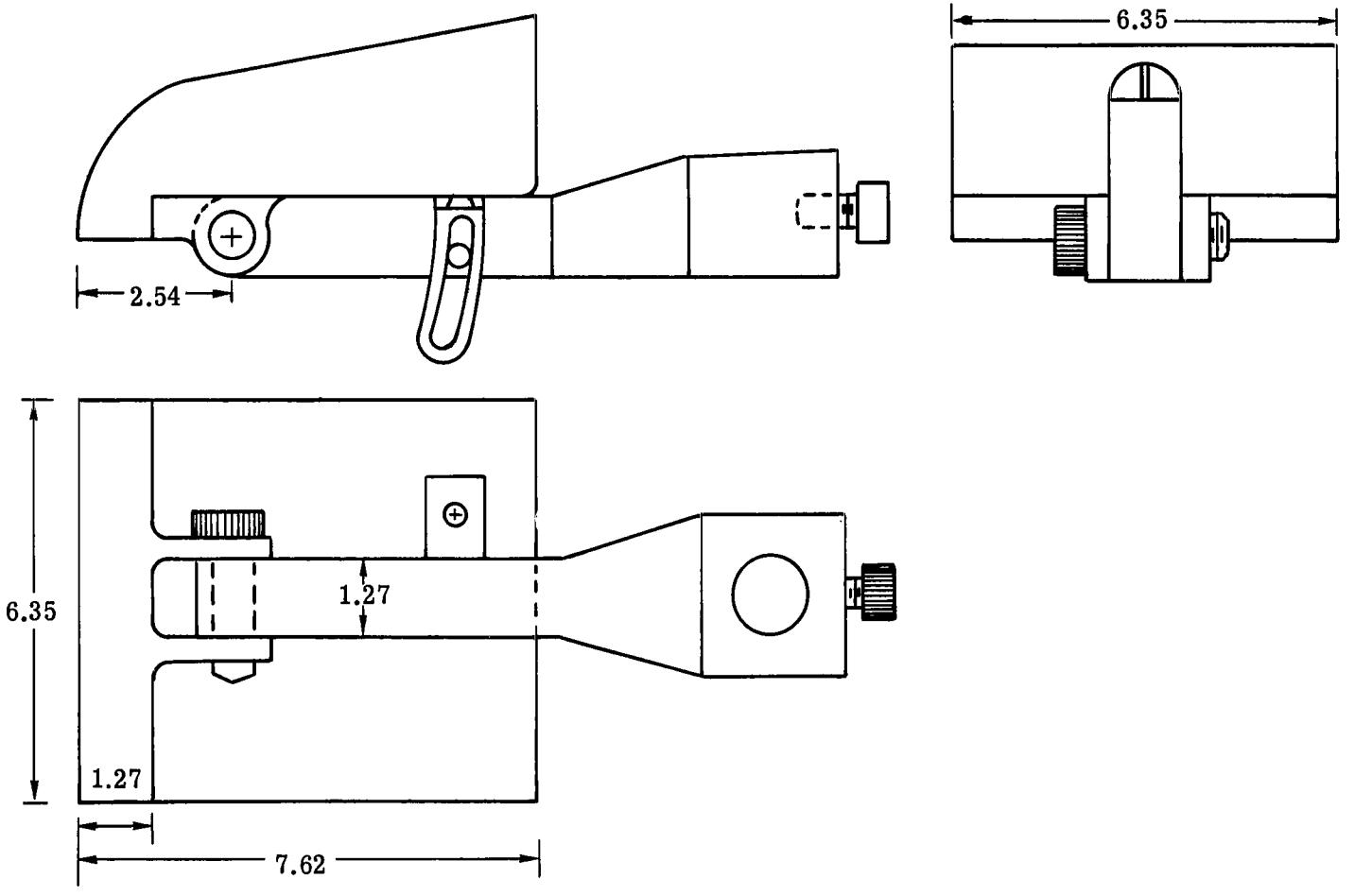

(b) Blunt-body model.

Figure 3.- Concluded.

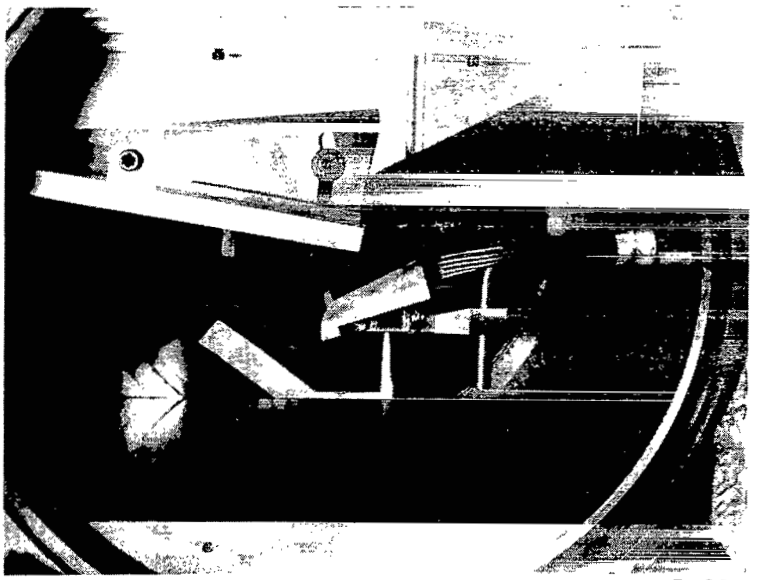

L-75-238

Figure 4.- Second set of models mounted in 11-inch tunnel test section.

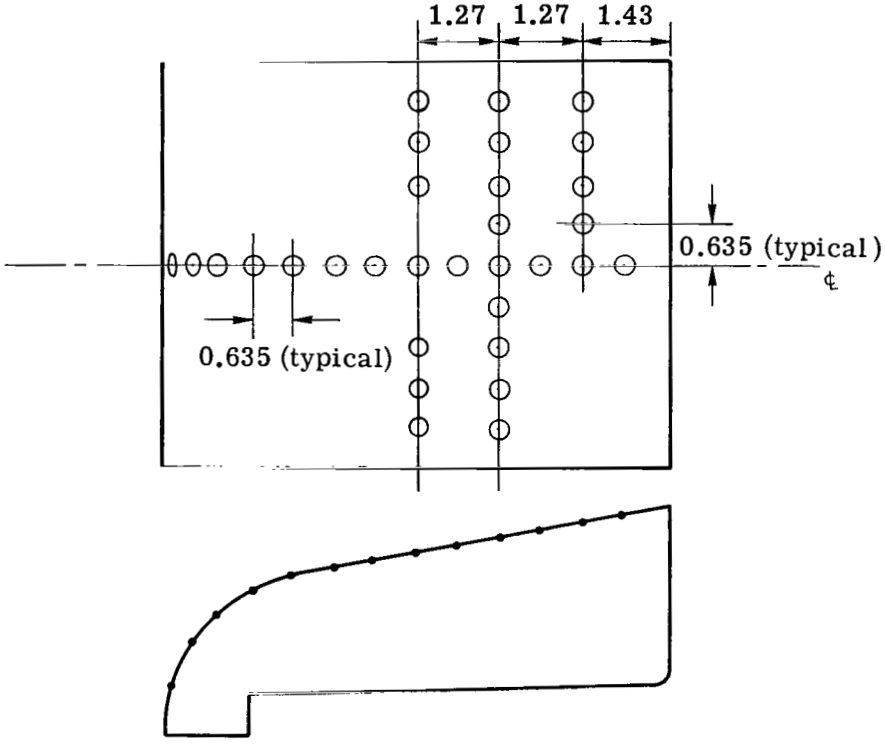

Figure 5.- Location of surface static-pressure orifices.
All dimensions are in cm.

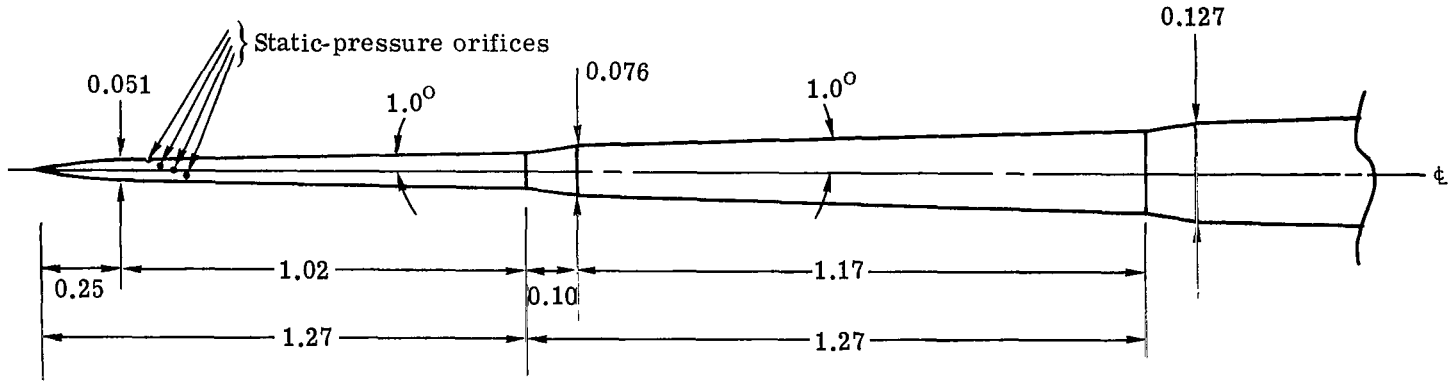

Figure 6.- Static-pressure probe (not to scale). Dimensions are in cm.

(a) 15° shock generator wedge; p_o = 10 atm.

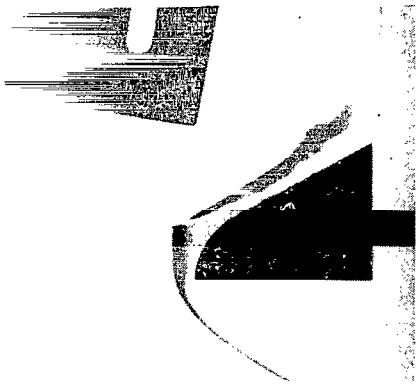

(b) 10° shock generator wedge; p_o = 10 atm.

(c) 10° shock generator wedge; bases of wedge and model alined; p_o = 15 atm.

L-75-239

Figure 7.- Schlieren photographs from preliminary studies in 11-inch tunnel.

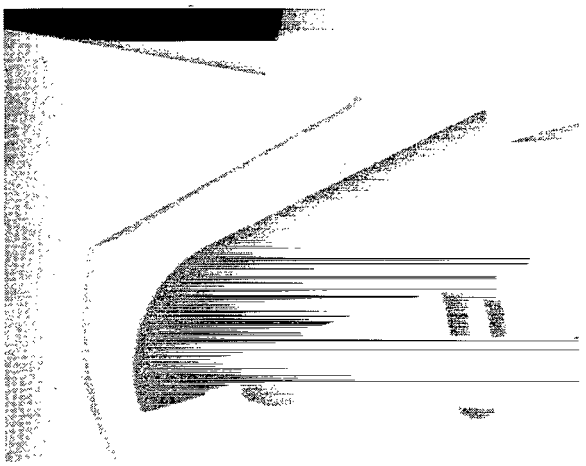

(a) p_o = 2.5 atm, 11-inch tunnel.

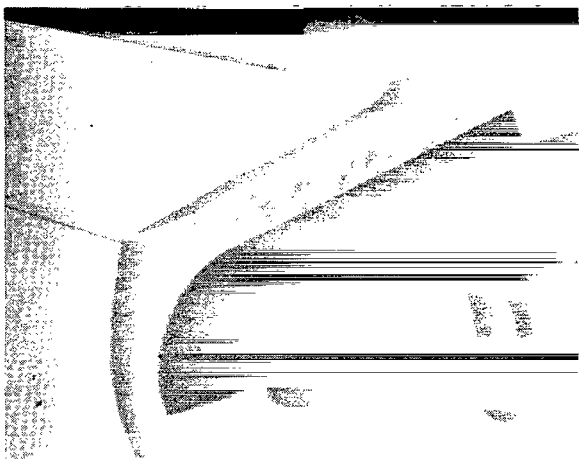

(b) p_o = 5 atm, 11-inch tunnel.

(c) p_o = 10 atm, 11-inch tunnel.

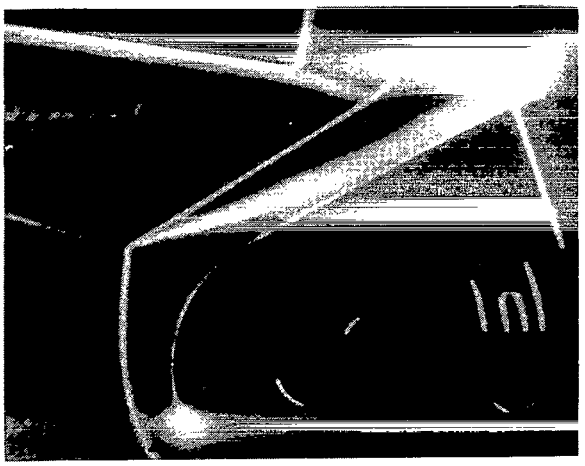

(d) p_o = 4.4 atm, 11-inch tunnel.

L-75-240

Figure 8.- Schlieren photographs of flow field for various unit Reynolds numbers.

L-75-241

(e) p_o = 1.03 MN/m^2, 20-inch tunnel.

Figure 8.- Continued.

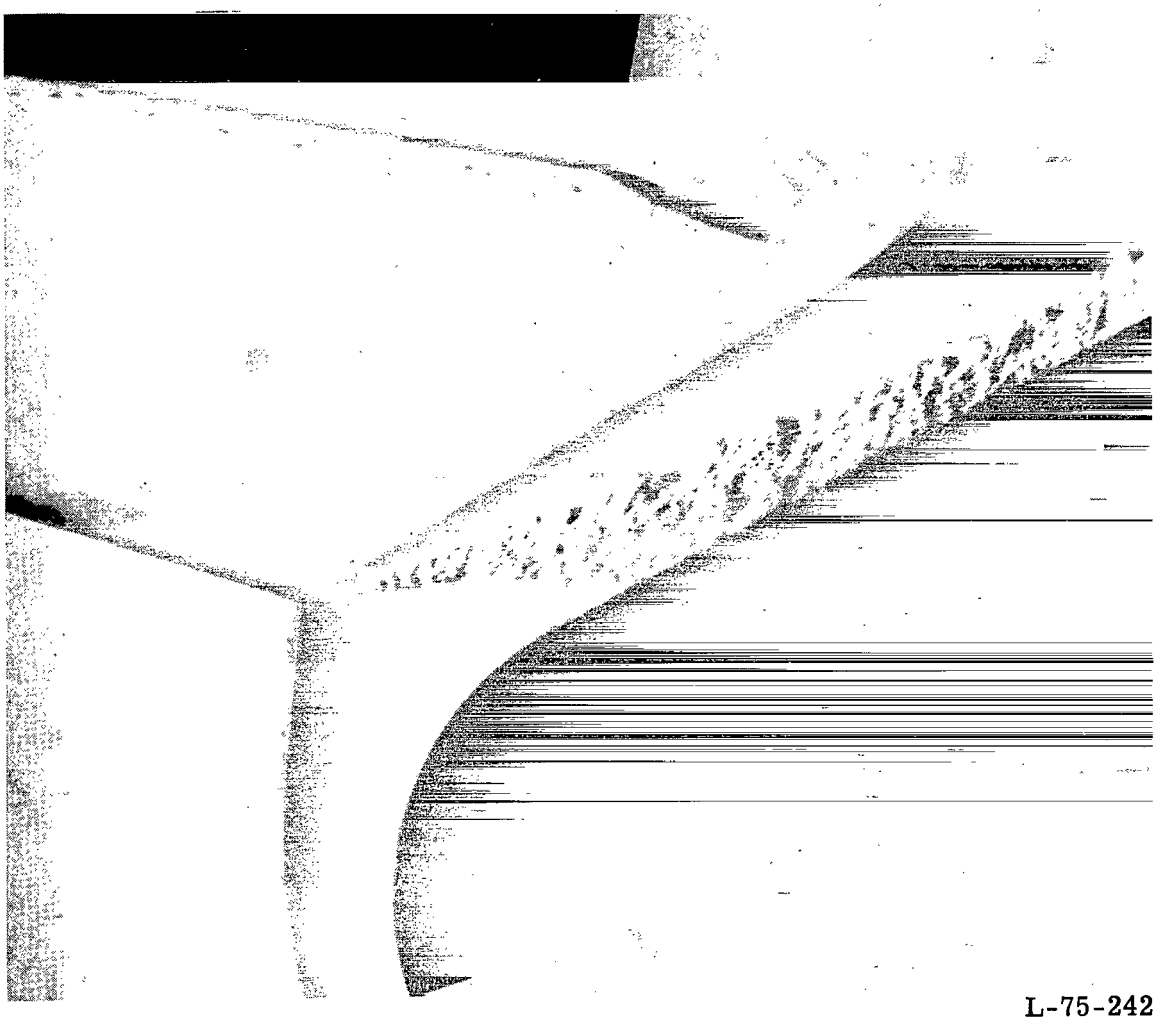

L-75-242

(f) p_o = 2.10 MN/m^2, 20-inch tunnel.

Figure 8.- Continued.

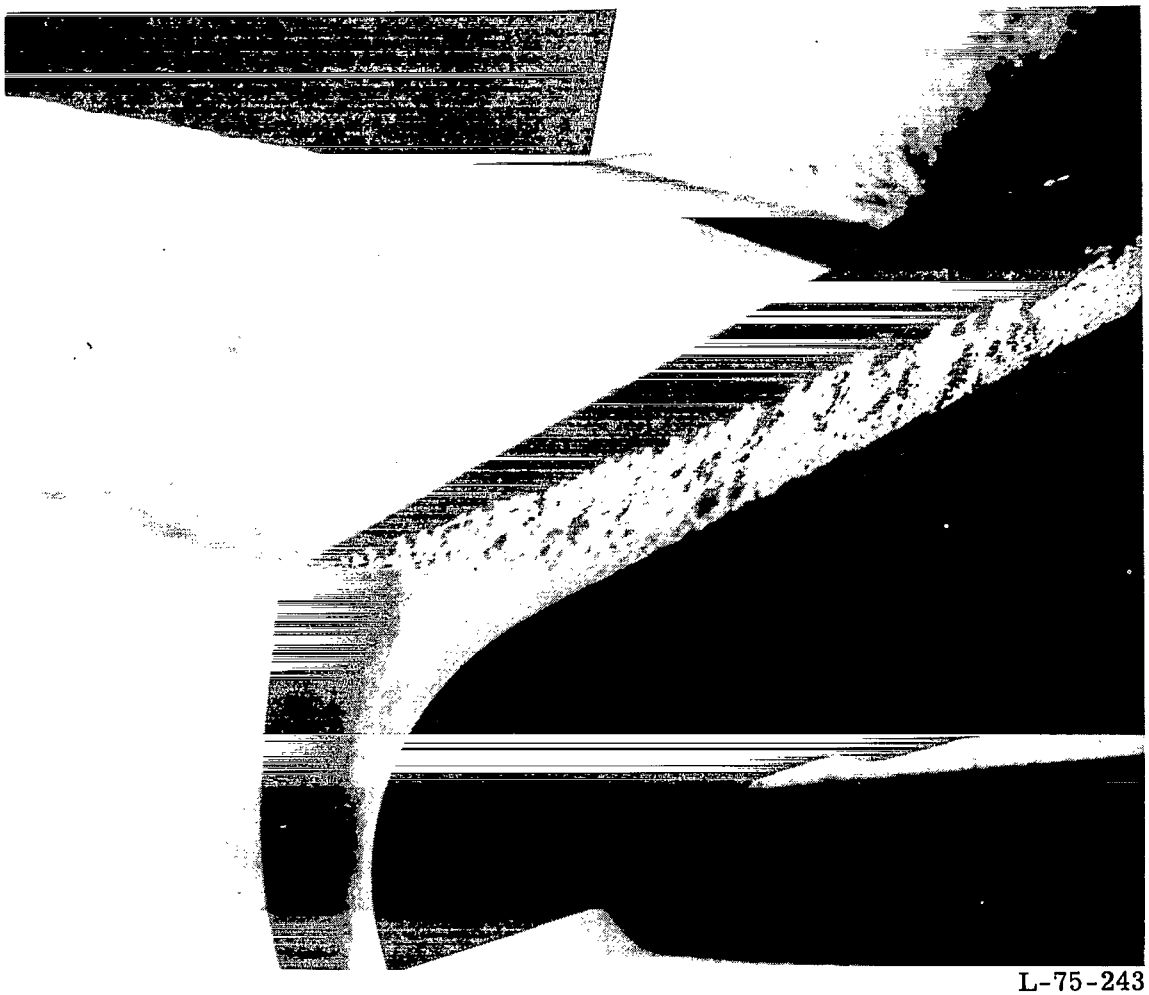

L-75-243

(g) p_o = 3.45 MN/m^2, 20-inch tunnel.

Figure 8.- Concluded.

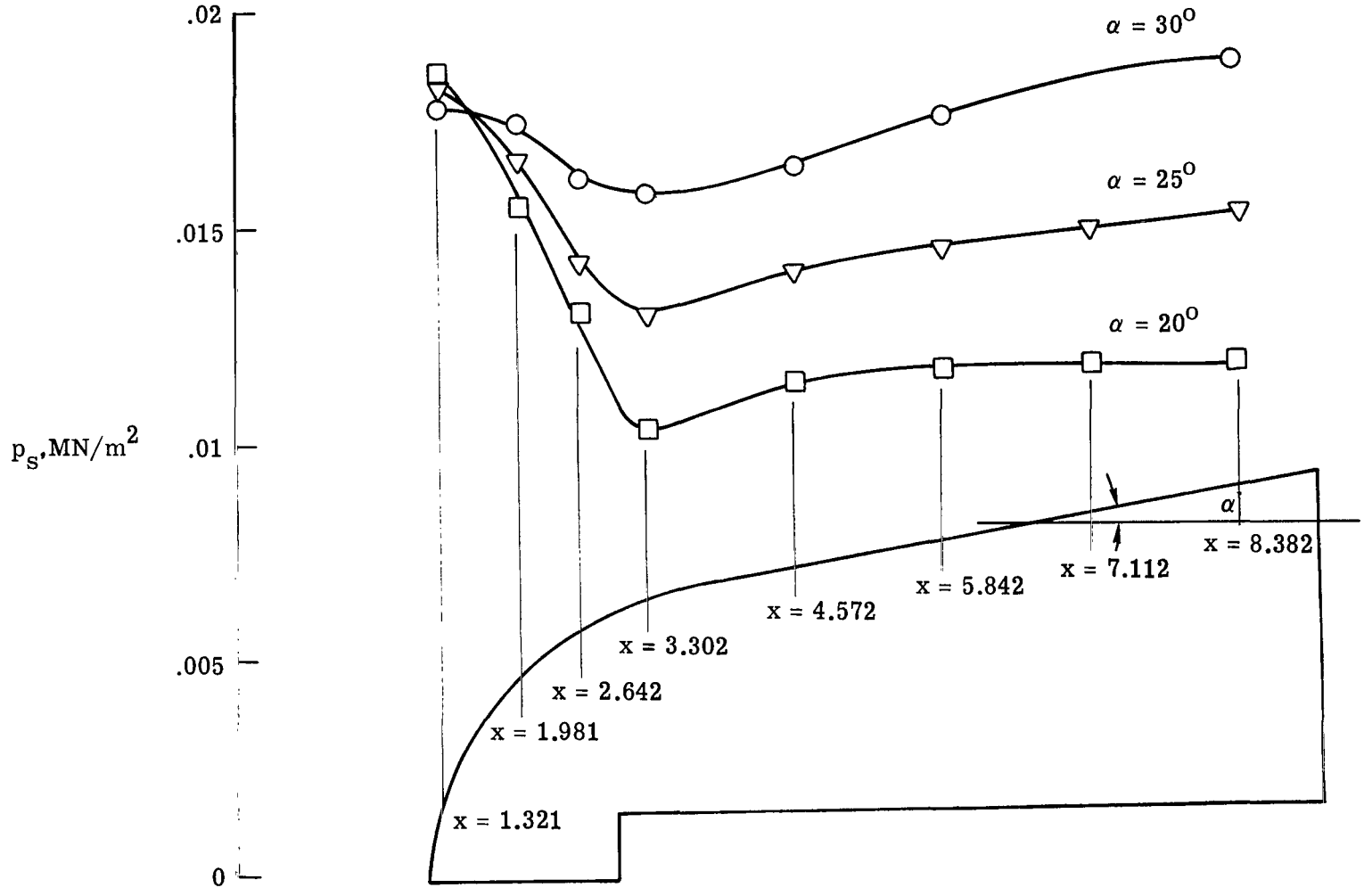

Figure 9.- Variation of center-line surface static pressure with angle of inclination of blunt-body model. p_o = 10 atm; 11-inch tunnel; x is given in cm.

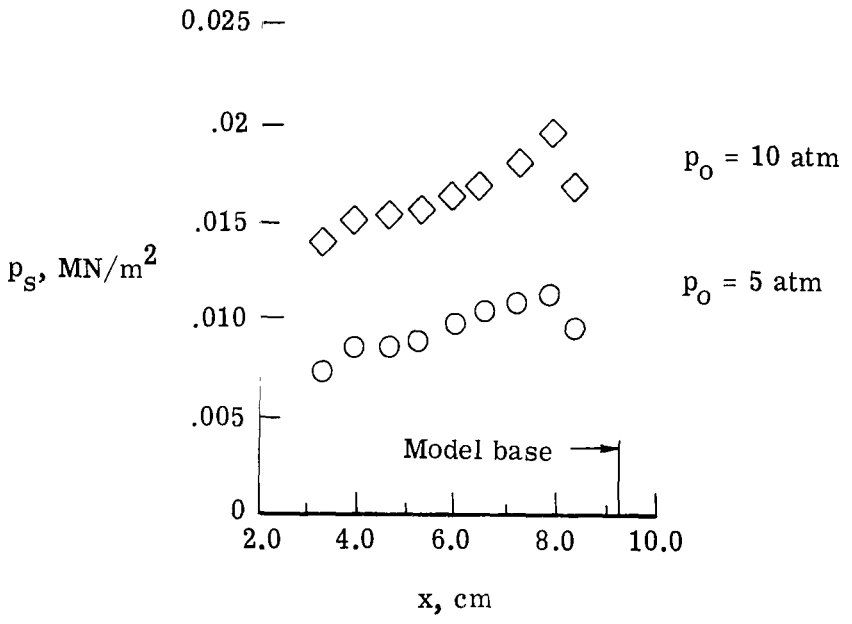

Figure 10.- Variation of center-line surface static pressure with tunnel total pressure. M_∞ = 6.7; 11-inch tunnel.

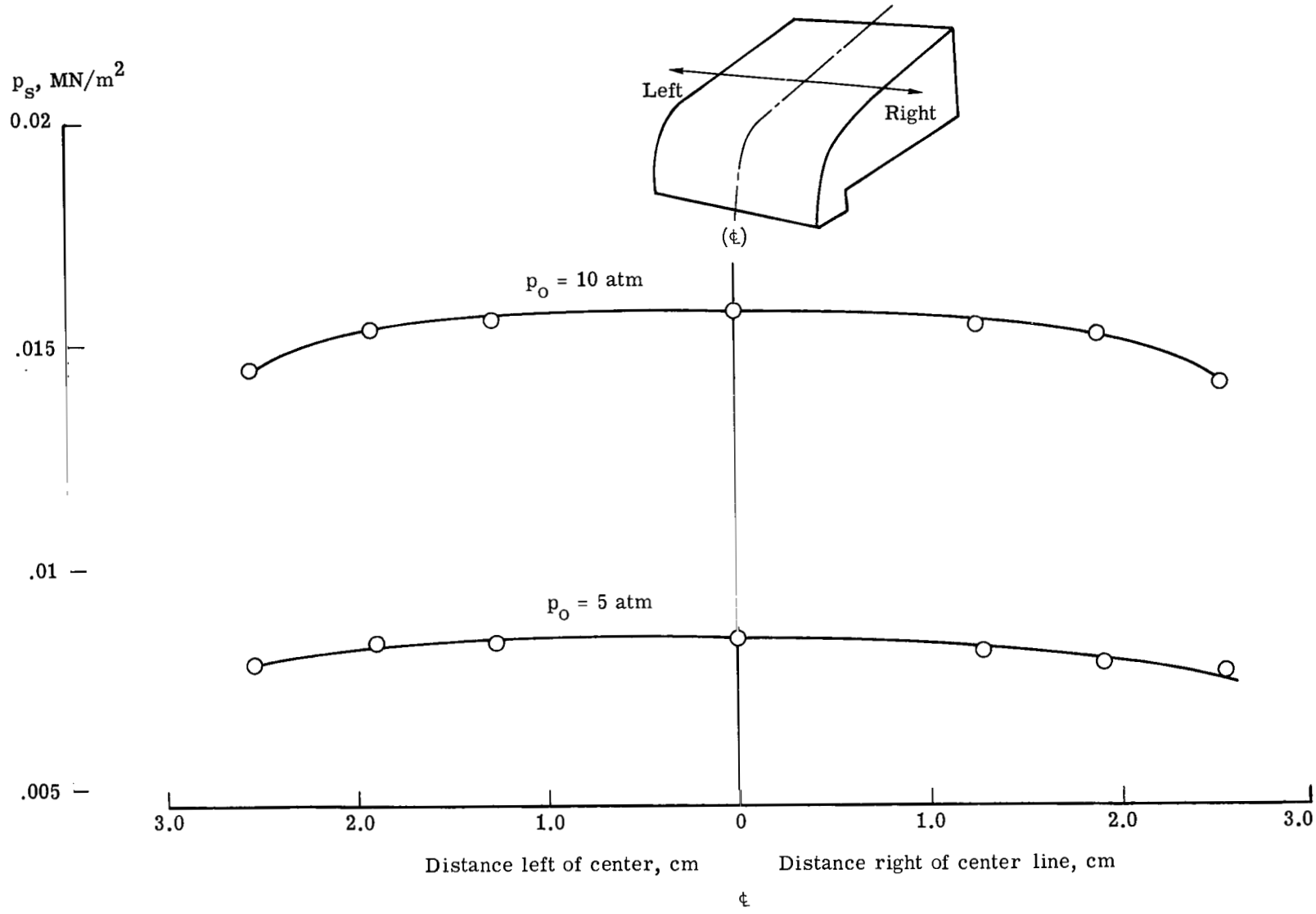

Figure 11.- Off-center-line surface static pressure at x = 5.21 cm.

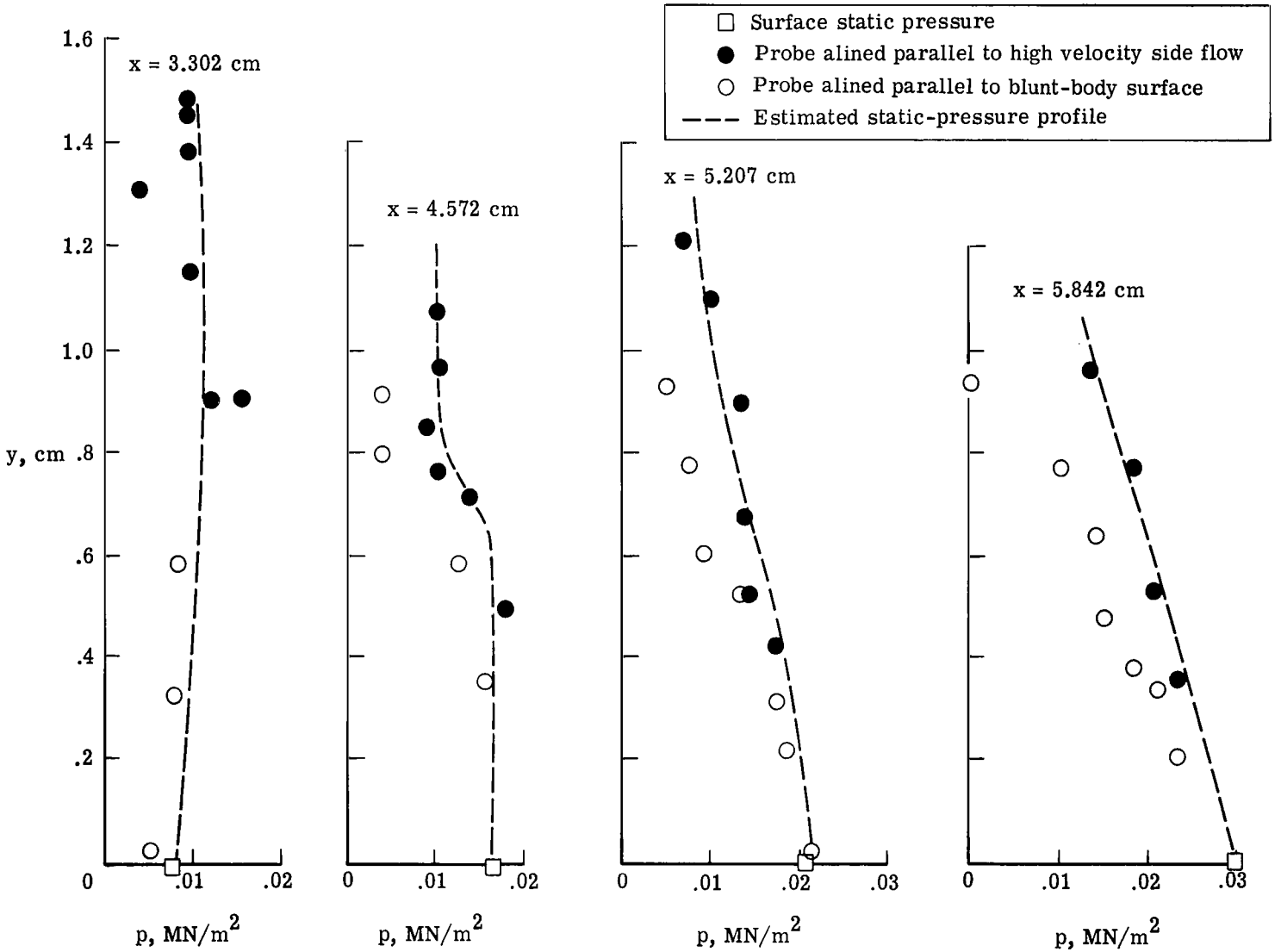

Figure 12.- Static-pressure profiles. 11-inch tunnel; p_o = 10 atm.

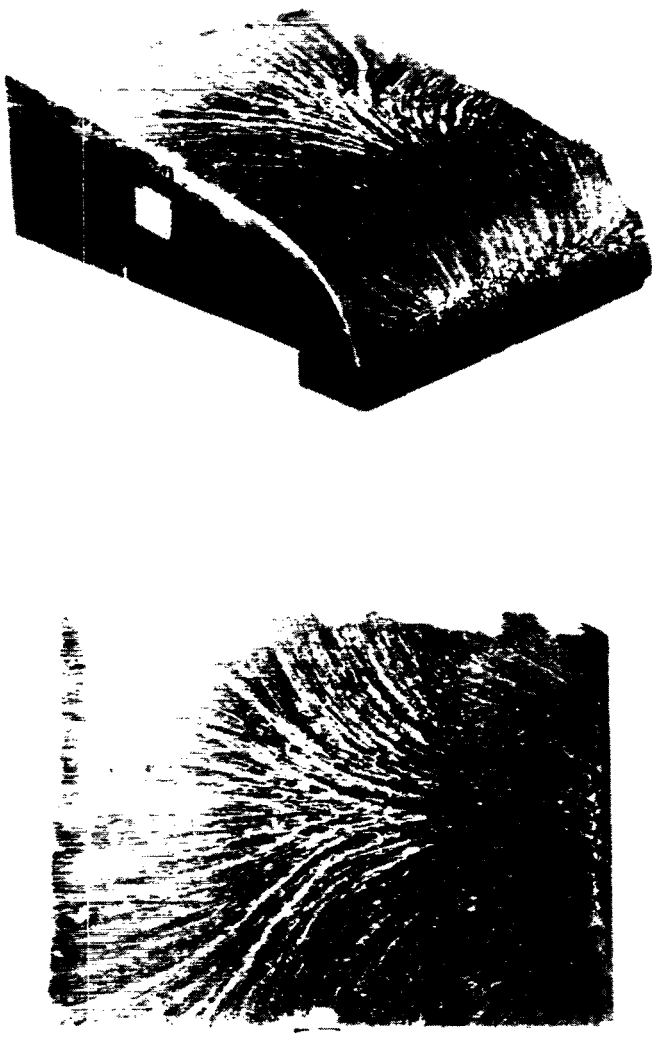

L-75-244

Figure 13.- Surface oil-flow pattern. p_o = 10 atm; 11-inch tunnel.

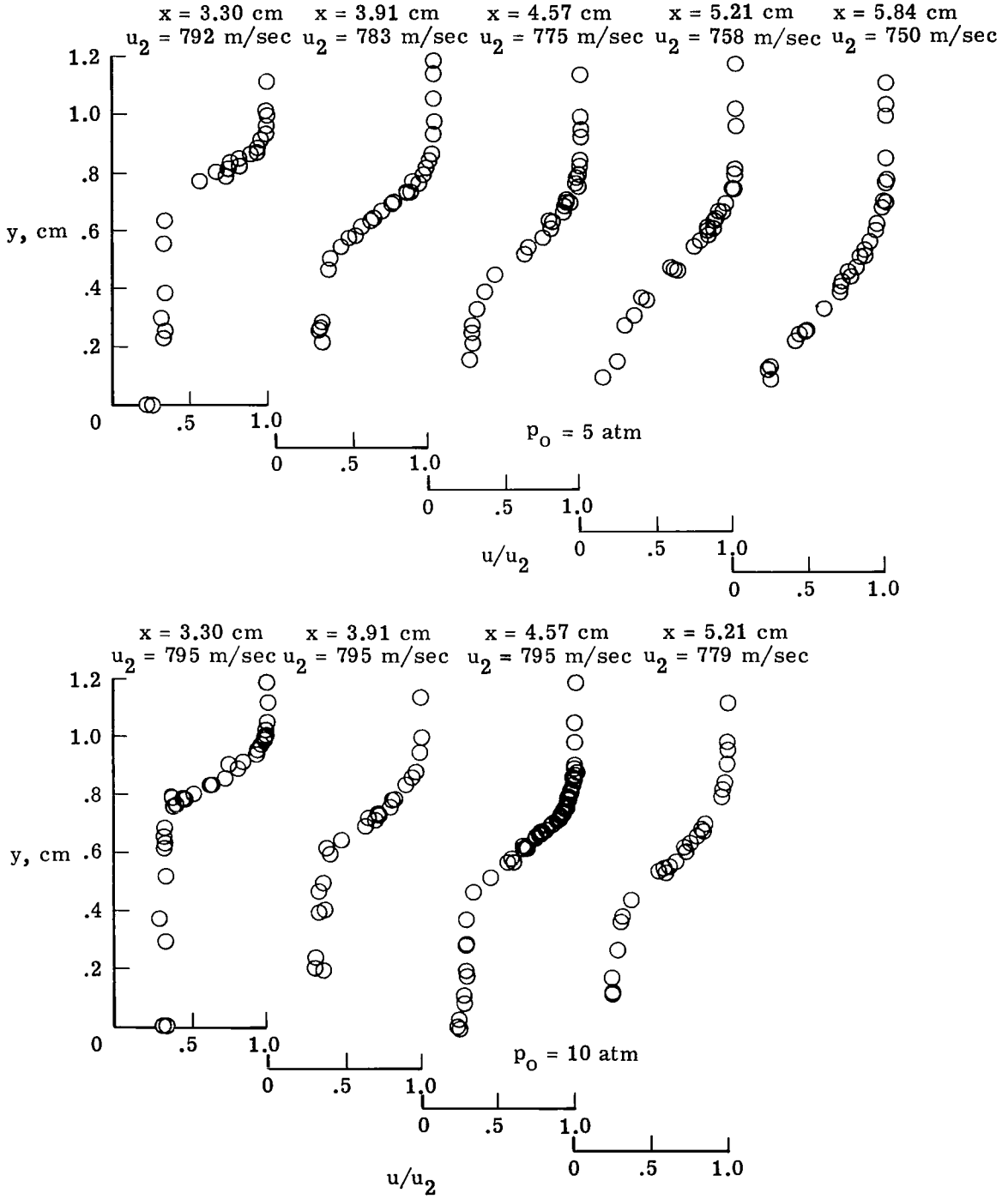

Figure 14.- Center-line mean velocity profiles. 11-inch tunnel tests.

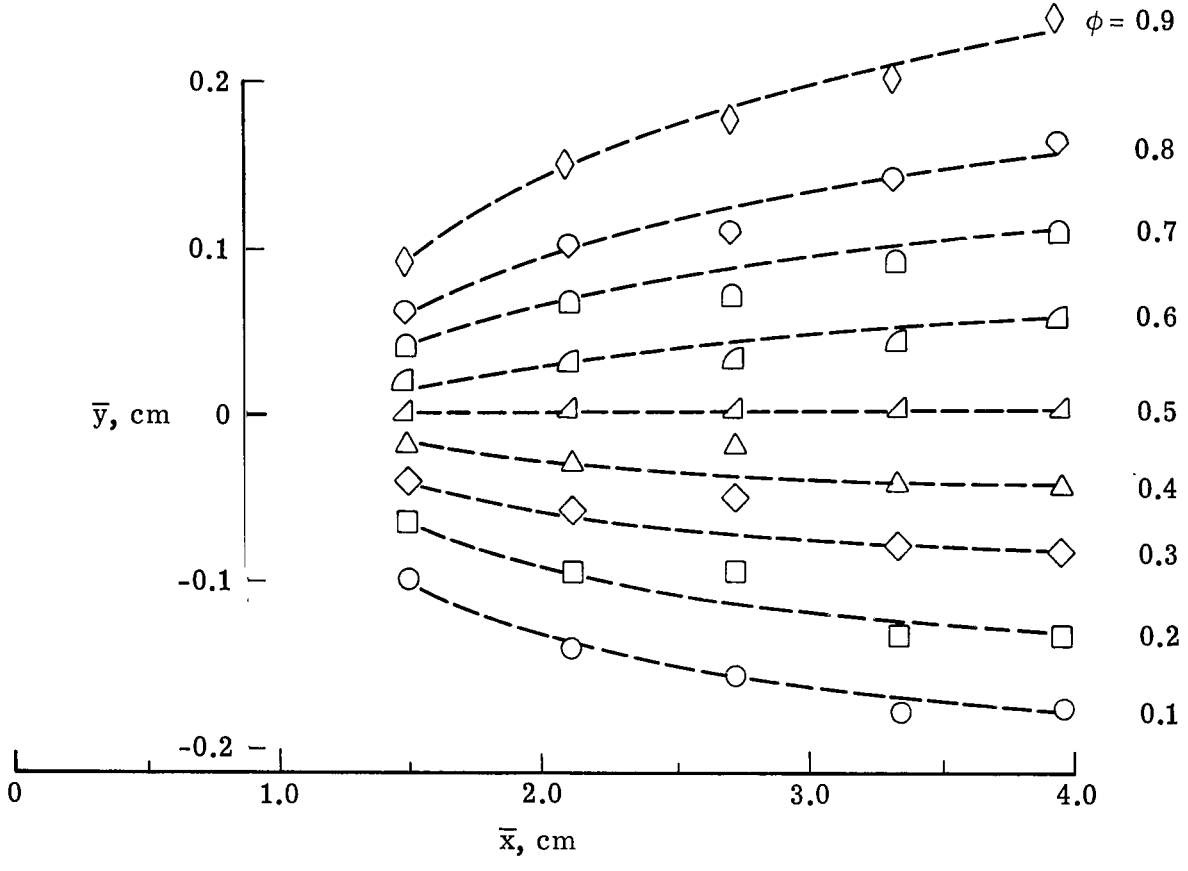

(a) p_o = 5 atm.

Figure 15.- Lines of constant ϕ. 11-inch tunnel results. Data points shown are interpolated points.

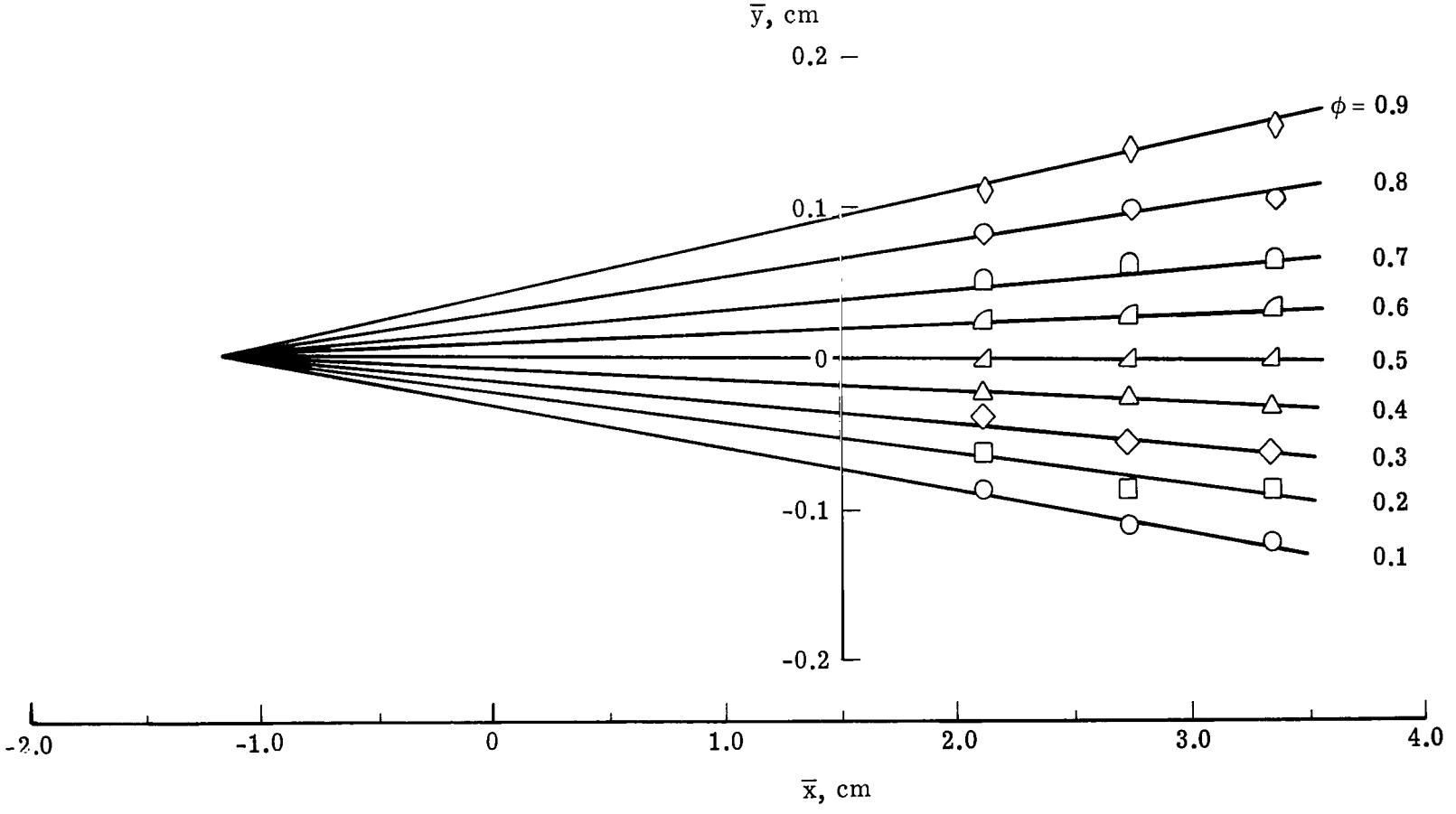

(b) p_o = 10 atm.

Figure 15.- Concluded.

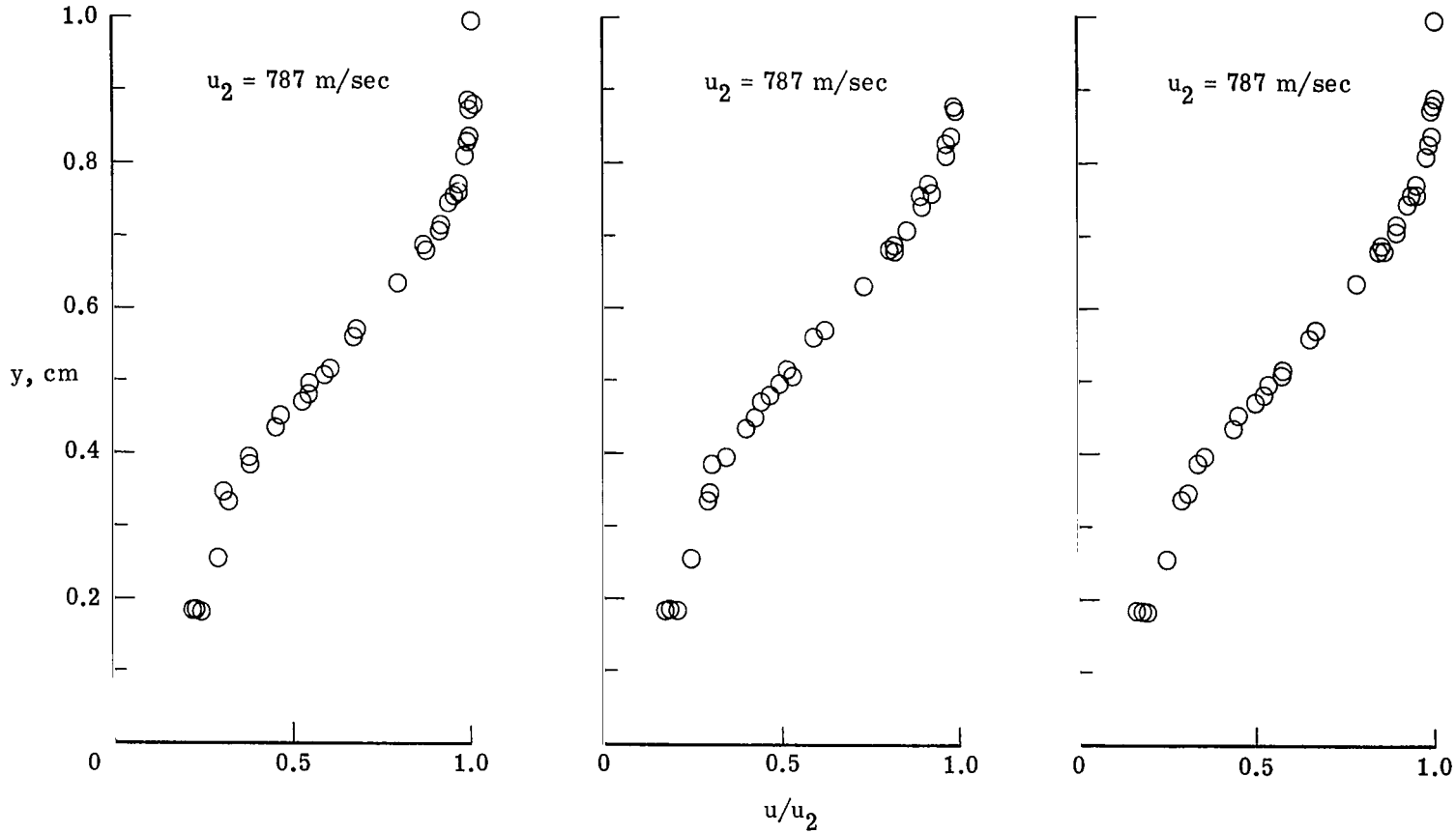

Profile 1.27 cm to left of center line

Center-line profile

Profile 1.27 cm to right of center line

Figure 16.- Off-center-line and center-line mean velocity profiles. x = 5.21 cm; p_o = 10 atm; 11-inch tunnel.

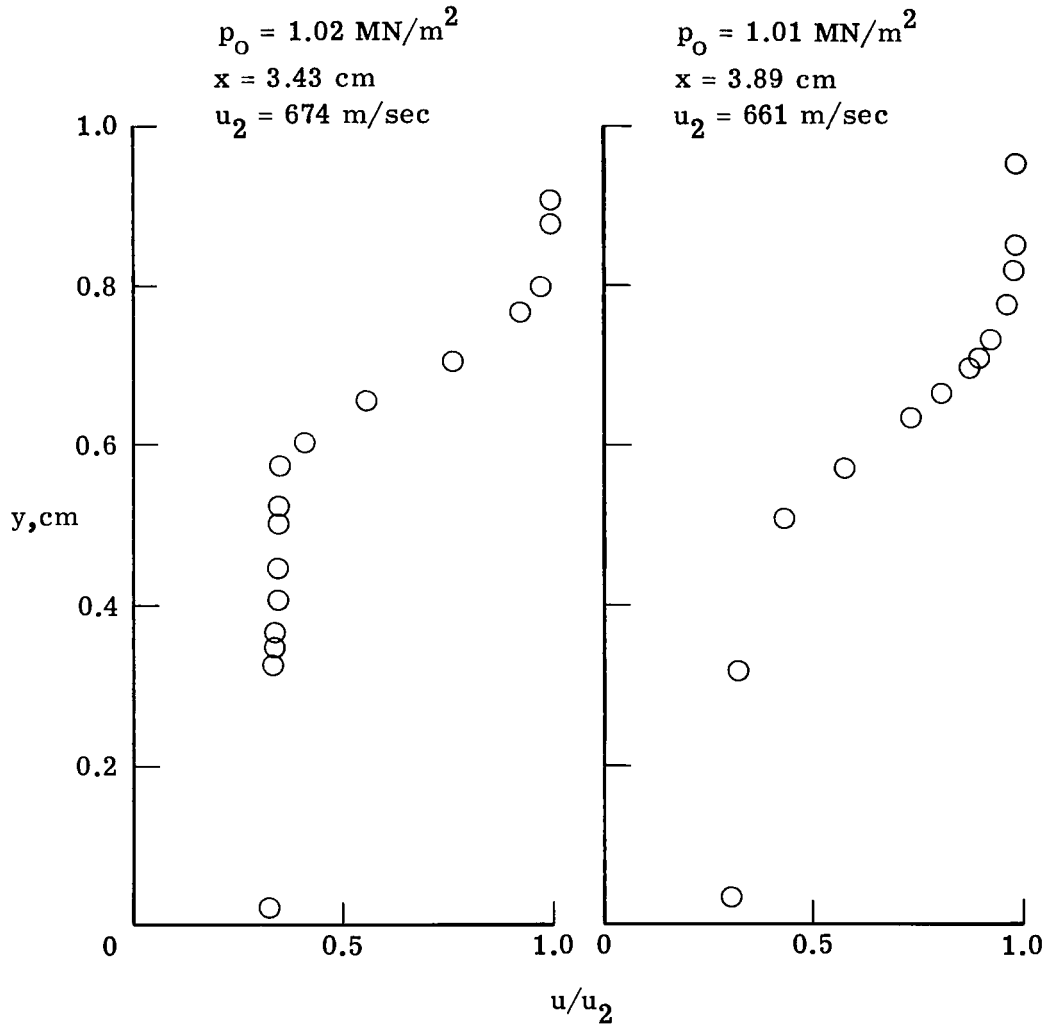

Figure 17.- Center-line mean velocity profiles. 20-inch tunnel; nominal p_o = 1.03 MN/m^2.

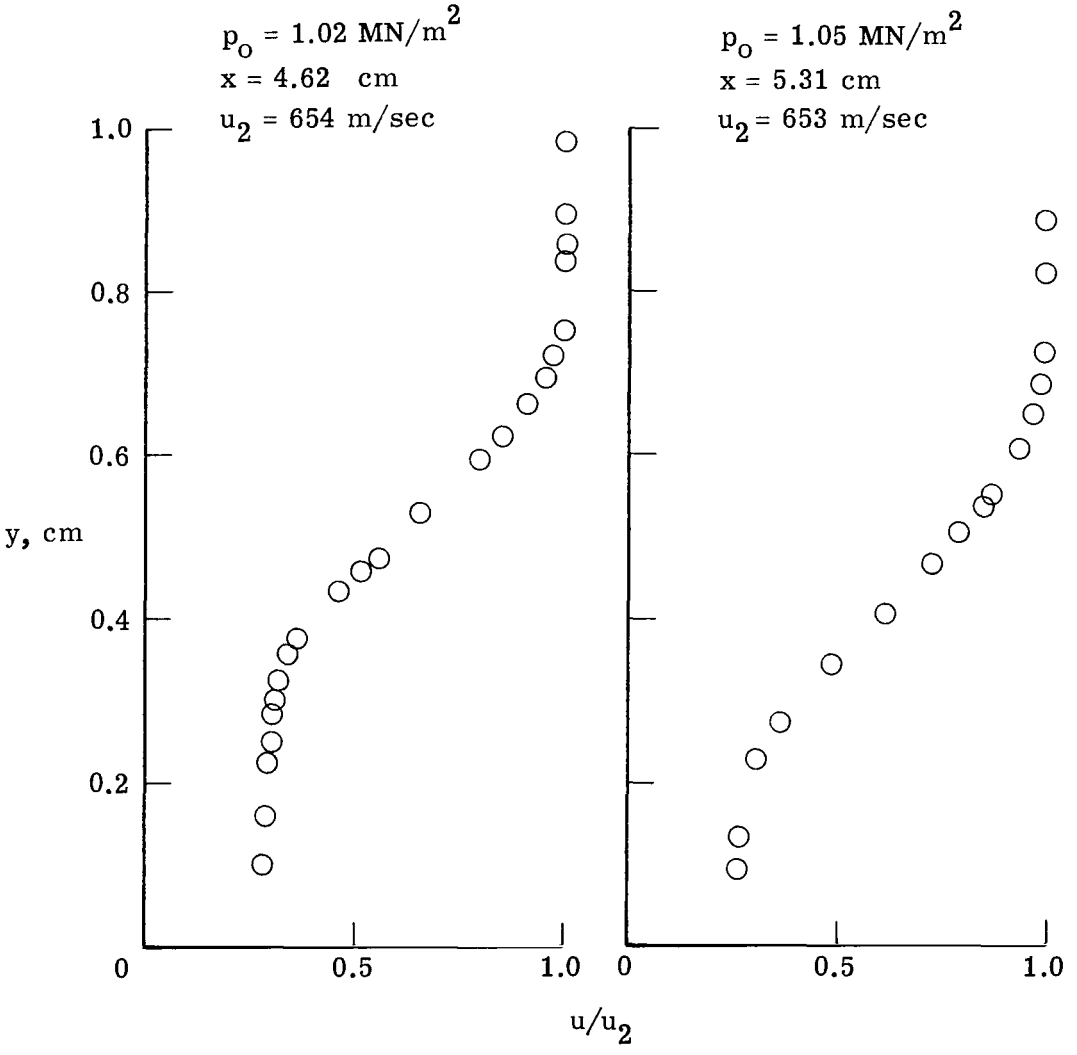

Figure 17.- Concluded.

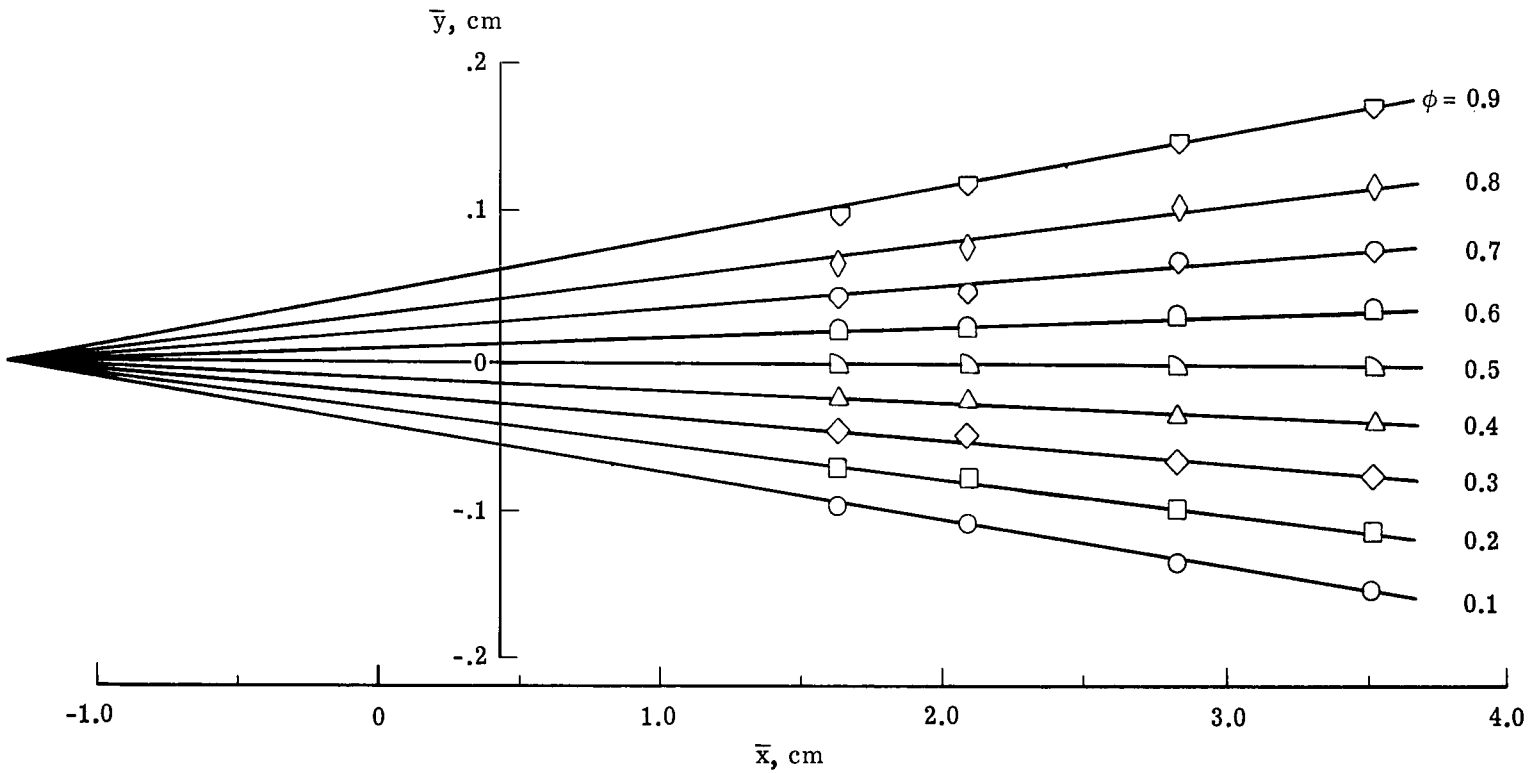

Figure 18.- Constant ϕ lines for 20-inch results. p_o = 1.03 MN/m^2.
Data points shown are interpolated points.

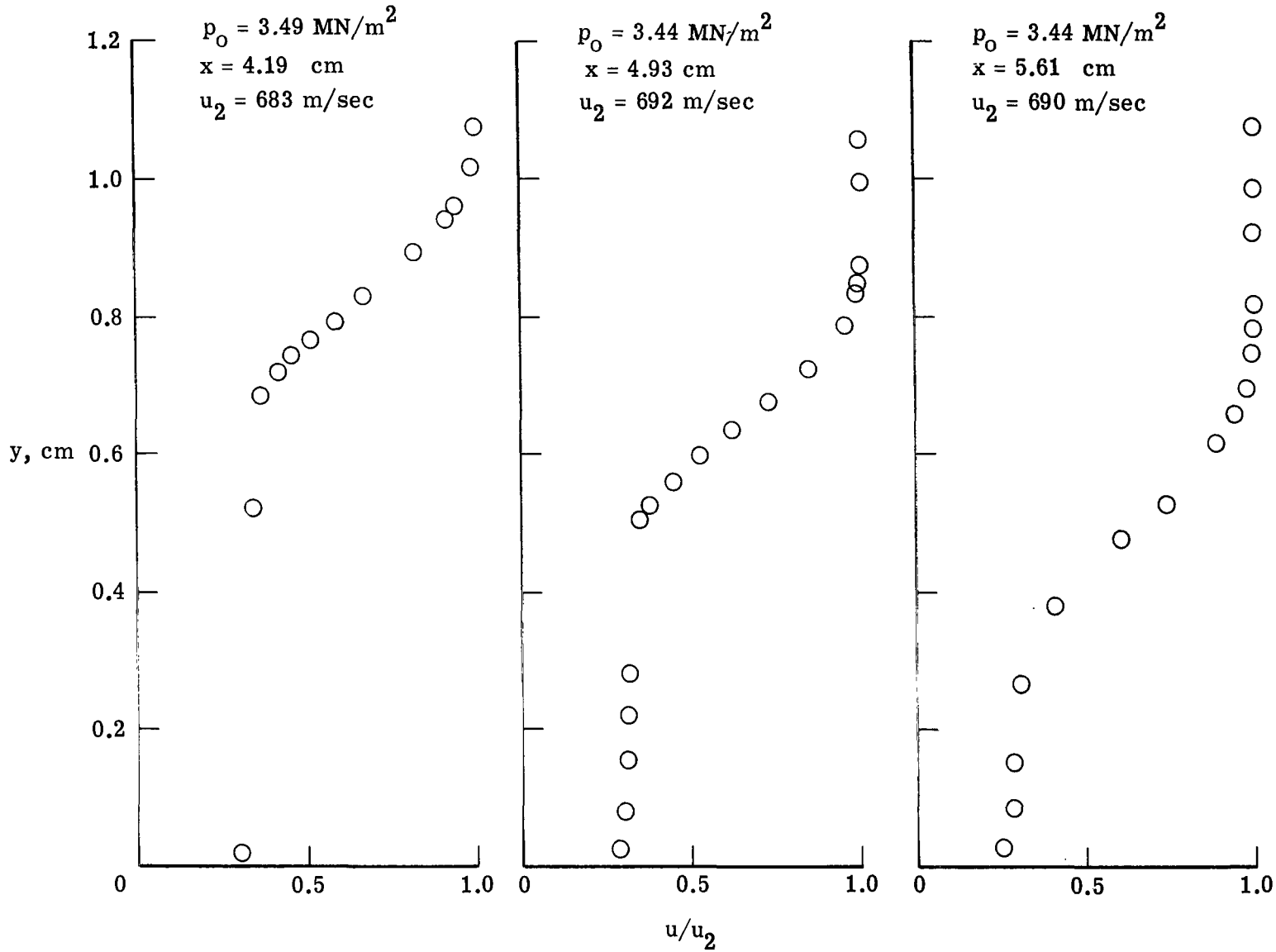

Figure 19.- Center-line mean velocity profiles. 20-inch tunnel; nominal p_o = 3.45 MN/m^2.

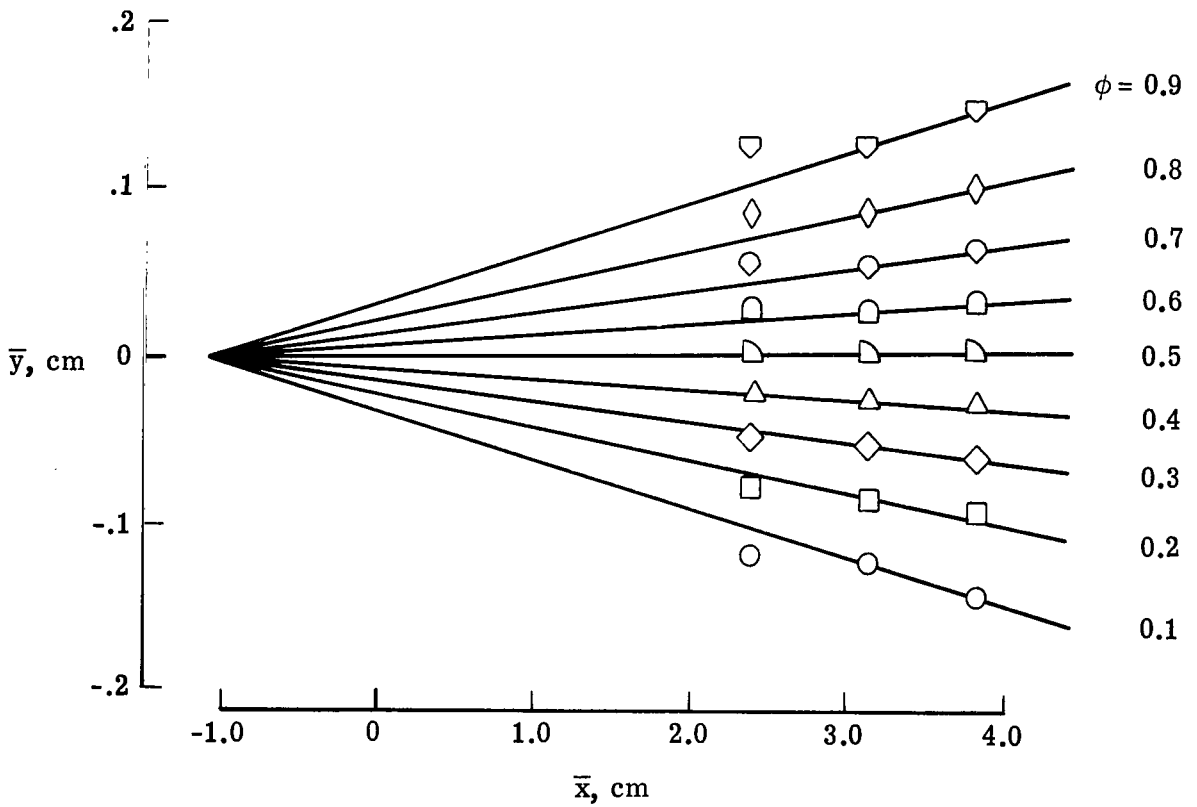

Figure 20.- Constant ϕ lines for 20-inch results. p_o = 3.45 MN/m^2.
Data points shown are interpolated points.

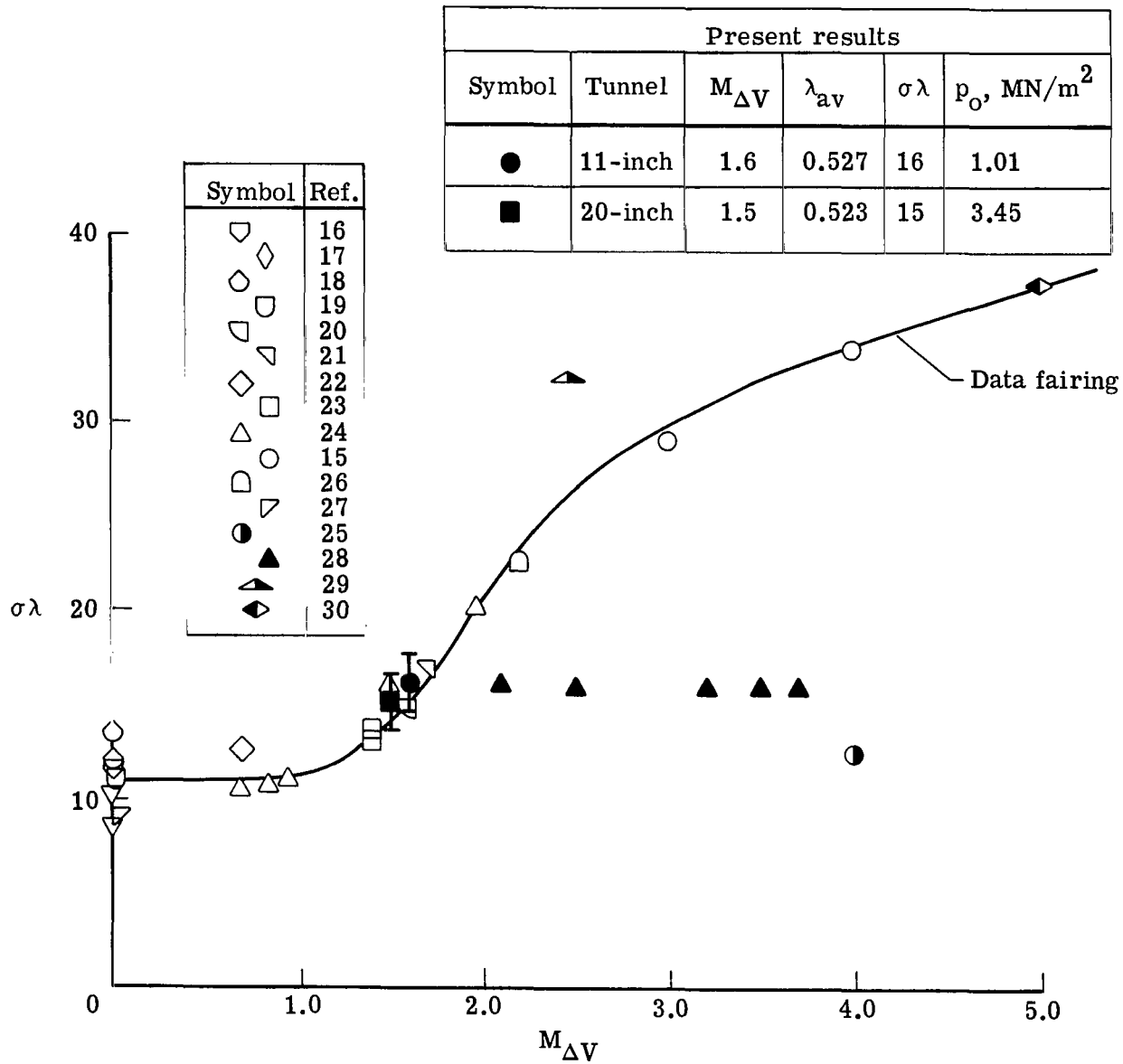

Figure 21.- Comparison of present results with other experimental data.

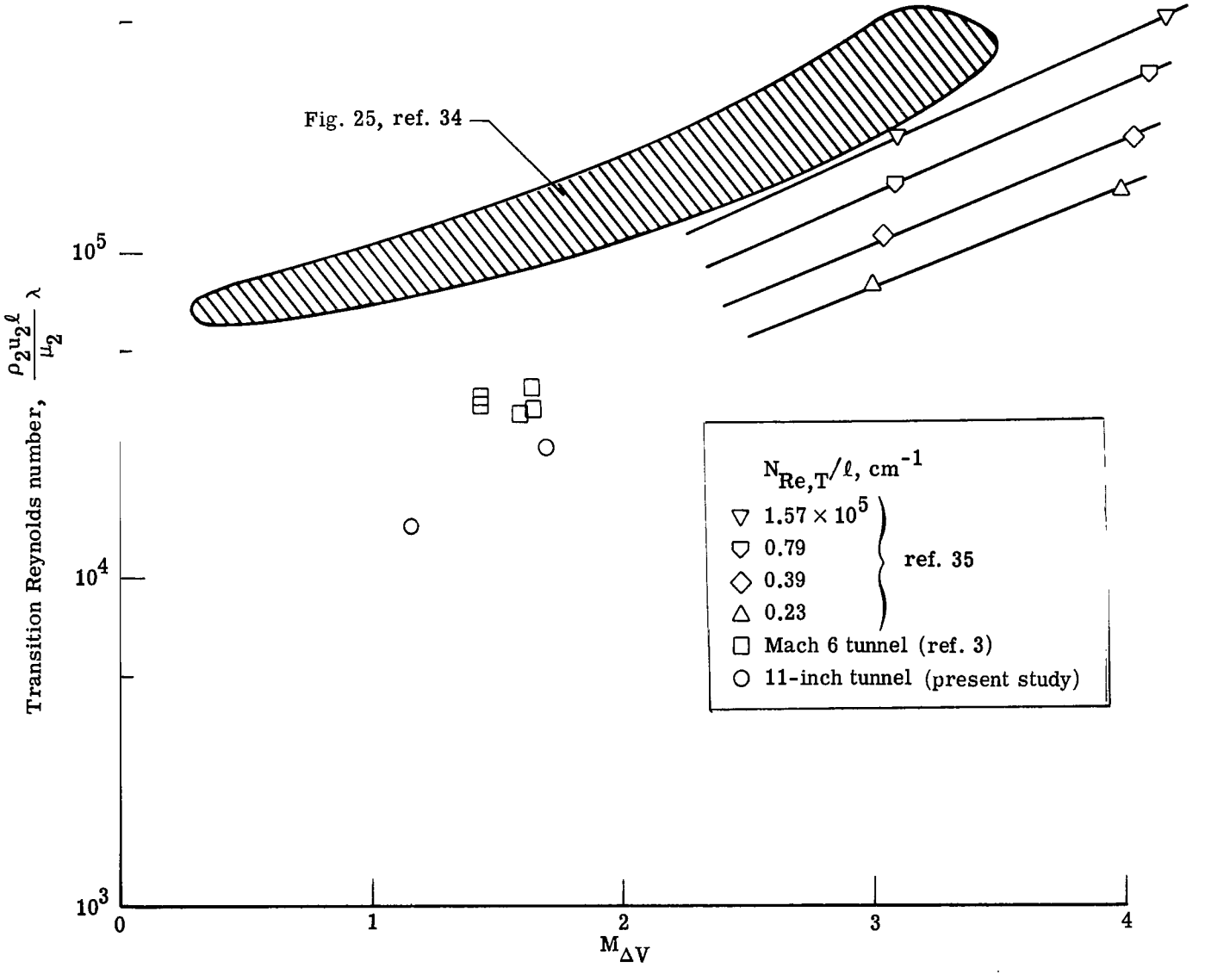

Figure 22.- Variation of transition Reynolds number with Mach number.

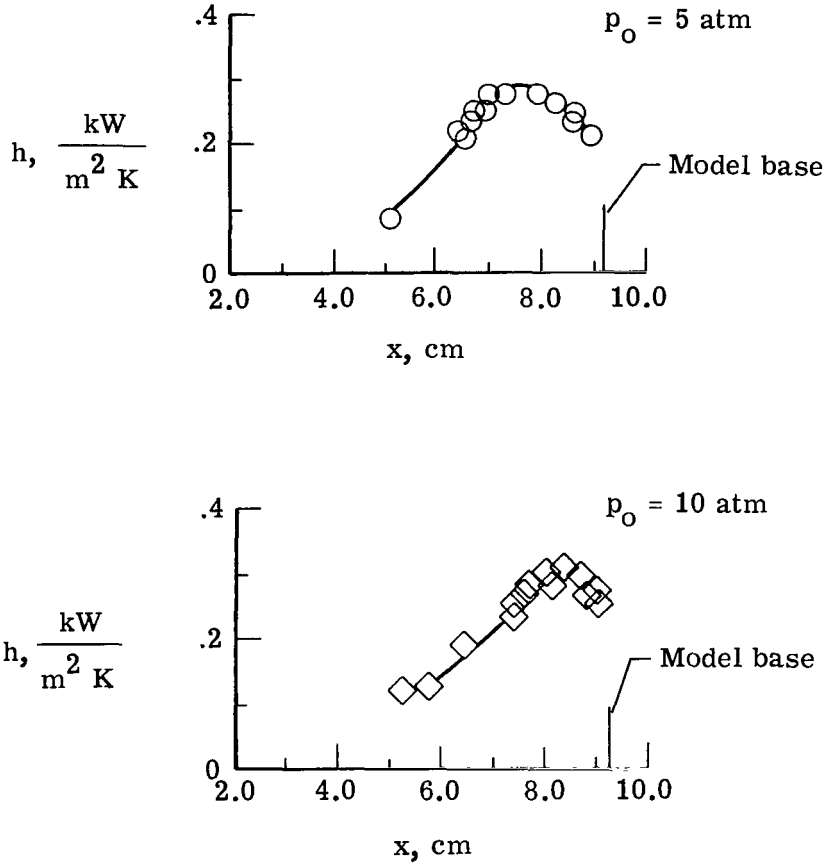

Figure 23.- Center-line surface heat transfer in the attachment region. 11-inch tunnel.

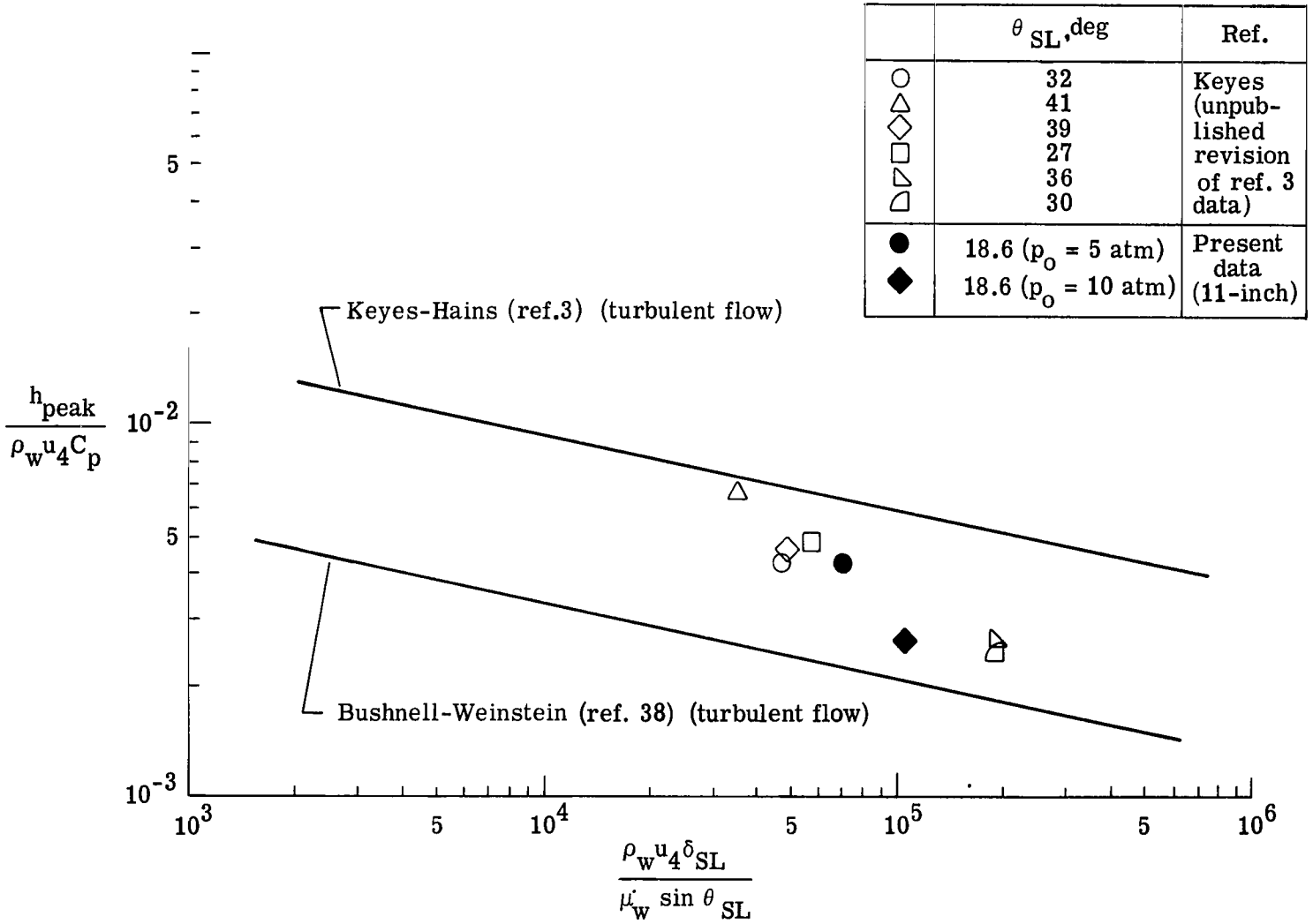

Figure 24.- Comparison of peak heat-transfer data with other data.

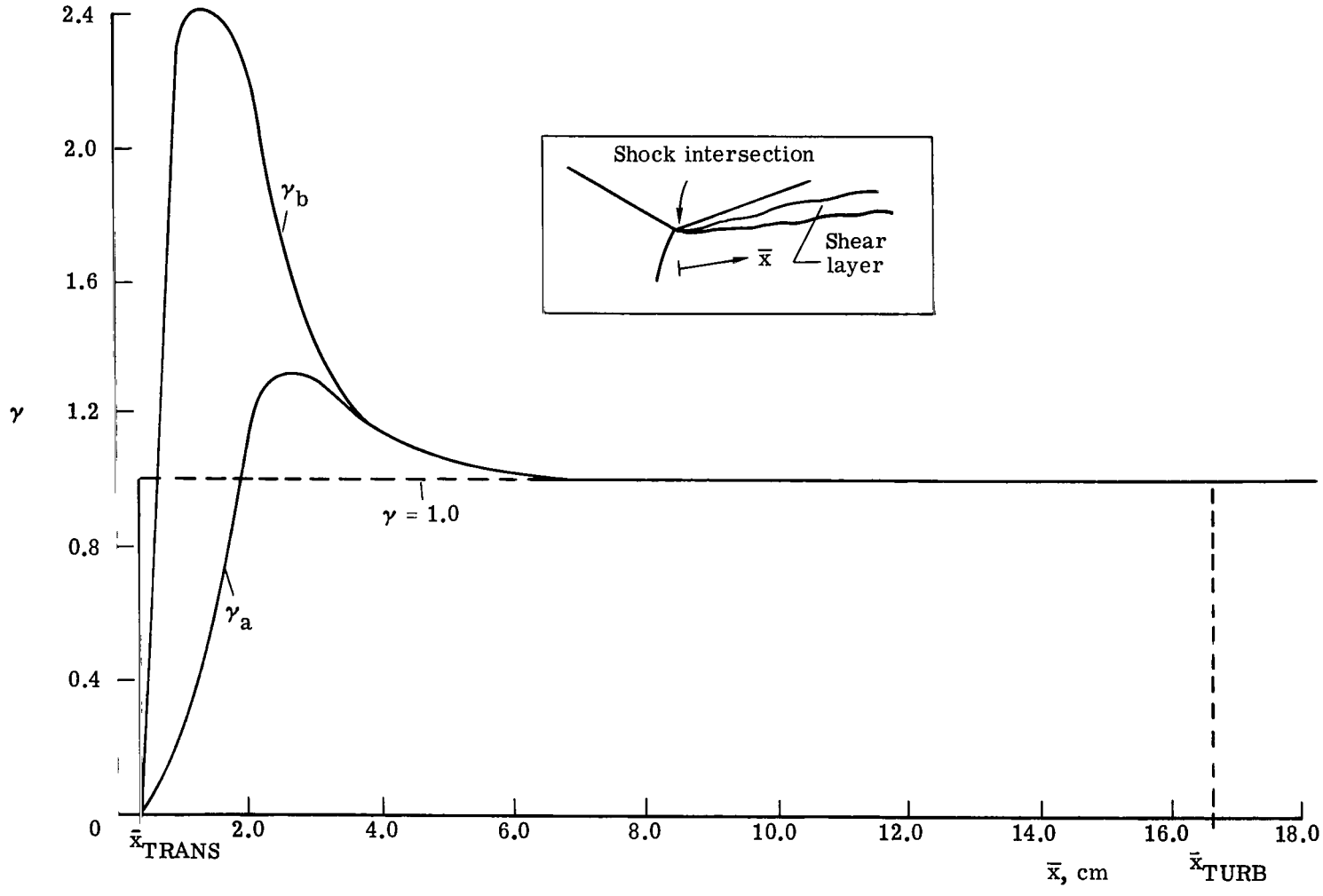

Figure 25.- Streamwise effective viscosity function.

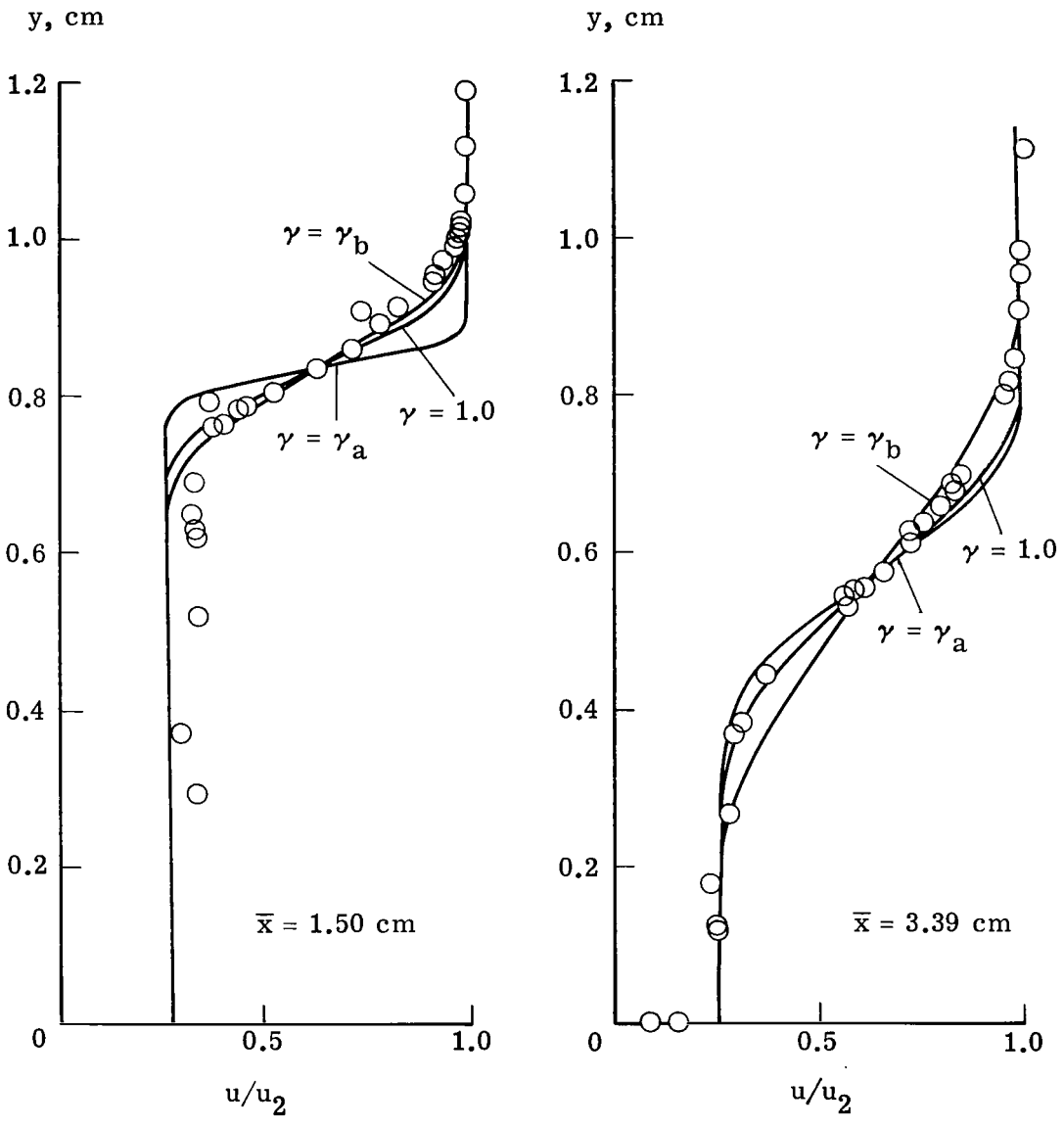

Figure 26.- Comparison of predicted profiles with experimental profiles for 11-inch results. p_o = 10 atm; ℓ/δ = 0.064.

"The aeronautical and space activities of the United States shall be conducted so as to contribute . . . to the expansion of human knowledge of phenomena in the atmosphere and space. The Administration shall provide for the widest practicable and appropriate dissemination of information concerning its activities and the results thereof."

—NATIONAL AERONAUTICS AND SPACE ACT OF 1958

NASA SCIENTIFIC AND TECHNICAL PUBLICATIONS

TECHNICAL REPORTS: Scientific and technical information considered important, complete, and a lasting contribution to existing knowledge.

TECHNICAL NOTES: Information less broad in scope but nevertheless of importance as a contribution to existing knowledge.

TECHNICAL MEMORANDUMS: Information receiving limited distribution because of preliminary data, security classification, or other reasons. Also includes conference proceedings with either limited or unlimited distribution.

CONTRACTOR REPORTS: Scientific and technical information generated under a NASA contract or grant and considered an important contribution to existing knowledge.

TECHNICAL TRANSLATIONS: Information published in a foreign language considered to merit NASA distribution in English.

SPECIAL PUBLICATIONS: Information derived from or of value to NASA activities. Publications include final reports of major projects, monographs, data compilations, handbooks, sourcebooks, and special bibliographies.

TECHNOLOGY UTILIZATION PUBLICATIONS: Information on technology used by NASA that may be of particular interest in commercial and other non-aerospace applications. Publications include Tech Briefs, Technology Utilization Reports and Technology Surveys.

Details on the availability of these publications may be obtained from:

SCIENTIFIC AND TECHNICAL INFORMATION OFFICE

NATIONAL AERONAUTICS AND SPACE ADMINISTRATION

Washington, D.C. 20546